Journal of Pharmaceutical Analysis 14 (2024) 225–243

Contents lists available at ScienceDirect

Journal of Pharmaceutical Analysis

journal homepage: www.elsevier.com/locate/jpa

Original article

Targeted metabolomics reveals the aberrant energy status in diabetic peripheral neuropathy and the neuroprotective mechanism of traditional Chinese medicine JinMaiTong

Bingjia Zhao [a, 1], Qian Zhang [a, 1], Yiqian He [a], Weifang Cao [b], Wei Song [c, **], Xiaochun Liang [a, *]

[a] Department of Traditional Chinese Medicine, Peking Union Medical College Hospital, Peking Union Medical College, Chinese Academy of Medical Sciences, Beijing, 100730, China
[b] Institute of Basic Medicine Sciences, Chinese Academy of Medical Sciences, Beijing, 100005, China
[c] Medical Research Center, Peking Union Medical College Hospital, Peking Union Medical College, Chinese Academy of Medical Sciences, Beijing, 100730, China

ARTICLE INFO

Article history:
Received 15 June 2023
Received in revised form
15 August 2023
Accepted 18 September 2023
Available online 21 September 2023

Keywords:
Diabetic peripheral neuropathy
JinMaiTong
Energy metabolism
Targeted metabolomics
Adenosine monophosphate-activated protein kinase

ABSTRACT

Diabetic peripheral neuropathy (DPN) is a common and devastating complication of diabetes, for which effective therapies are currently lacking. Disturbed energy status plays a crucial role in DPN pathogenesis. However, the integrated profile of energy metabolism, especially the central carbohydrate metabolism, remains unclear in DPN. Here, we developed a metabolomics approach by targeting 56 metabolites using high-performance ion chromatography-tandem mass spectrometry (HPIC-MS/MS) to illustrate the integrative characteristics of central carbohydrate metabolism in patients with DPN and streptozotocin-induced DPN rats. Furthermore, JinMaiTong (JMT), a traditional Chinese medicine (TCM) formula, was found to be effective for DPN, improving the peripheral neurological function and alleviating the neuropathology of DPN rats even after demyelination and axonal degeneration. JMT ameliorated DPN by regulating the aberrant energy balance and mitochondrial functions, including excessive glycolysis restoration, tricarboxylic acid cycle improvement, and increased adenosine triphosphate (ATP) generation. Bioenergetic profile was aberrant in cultured rat Schwann cells under high-glucose conditions, which was remarkably corrected by JMT treatment. *In-vivo* and *in-vitro* studies revealed that these effects of JMT were mainly attributed to the activation of adenosine monophosphate (AMP)-activated protein kinase (AMPK) and downstream peroxisome proliferator-activated receptor gamma coactivator 1-alpha (PGC-1α). Our results expand the therapeutic framework for DPN and suggest the integrative modulation of energy metabolism using TCMs, such as JMT, as an effective strategy for its treatment.

1. Introduction

Diabetic peripheral neuropathy (DPN) is a common and severe complication of diabetes that is characterized by demyelination and axonal degeneration of peripheral nerves and affects at least half of all patients with diabetes [1–3]. Typical symptoms of DPN include neuropathic pain, dysesthesia (burning or tingling), numbness, weakness, and balance problems, resulting in a poor quality of life. Loss of sensation in the lower extremities also increases the risk of foot ulceration and limb amputation, resulting in high medical costs [4] and prolonged suffering for the patients. Other than optimal glycemic control, no specific treatments are currently available for peripheral nerve injuries caused by diabetes. Even strict glycemic control cannot completely block or reverse the progression of DPN. Therefore, effective DPN treatment is a significant challenge in clinical practice. The pathogenesis of DPN is complex and involves multiple mechanisms, including the activation of polyol pathway, accumulation of advanced glycation end products, oxidative stress, and inflammation [3,5].

Energy metabolism disorders and mitochondrial dysfunction play vital roles in the pathogenesis of DPN [6–8]. Central carbohydrate

Peer review under responsibility of Xi'an Jiaotong University.
* Corresponding author.
** Corresponding author.
E-mail addresses: Xiaochun_Liang@yeah.net (X. Liang), sw-yy1990@163.com (W. Song).
[1] Both authors contributed equally to this work.

https://doi.org/10.1016/j.jpha.2023.09.007

metabolism is considered as the core of energy metabolism, which mainly comprises the glycolysis (an anaerobic process that breaks 6-carbon glucose into 3-carbon pyruvate), tricarboxylic acid (TCA) cycle (also known as the citric acid cycle or Krebs cycle to produce adenosine triphosphate (ATP), and pentose phosphate (another pathway for glucose catabolism that produces reduced form of the nicotinamide adenine dinucleotide phosphate (NADPH)) pathways [9]. Chronic hyperglycemia can lead to elevated glycolysis and disturbances in the TCA cycle, resulting in axonal degeneration and demyelination of peripheral nerves [10–12]. However, owing to the structural similarity and hydrophilic nature of metabolites involved in central carbohydrate metabolism, the holistic view and bioenergetic crosstalk of these metabolic pathways in the circulation and peripheral nervous system have not yet been fully elucidated under the pathological condition of DPN. Therefore, a comprehensive understanding of metabolic profiles and underlying mechanisms of energy metabolism is crucial for the development of new therapeutic strategies for DPN.

The homeostatic control of energy balance involves a complex network of mediators and multiple signaling pathways. Mitochondria are the powerhouse of cells and play a key role in maintaining energy homeostasis. Accumulating evidence suggests that mitochondrial dysfunction in the peripheral nervous system plays a vital role in DPN [6,13–15]. Alterations in the ultrastructural morphology and proteome of mitochondria have been observed in both dorsal root ganglia (DRG) neurons and sciatic nerves of diabetic rodent models, as well as in cultured Schwann cells exposed to high glucose [14,16,17]. Furthermore, the activation of adenosine monophosphate (AMP)-activated protein kinase (AMPK), the master regulator of cellular energy homeostasis, was found to be depressed during diabetes [7]. The downstream peroxisome proliferator-activated receptor gamma coactivator 1-alpha (PGC-1α), a main mediator in coordinating mitochondrial biogenesis, has been proposed as a key factor for neuronal survival and synaptic transmission [18,19]. The disruption of AMPK/PGC-1α axis led to abnormal mitochondrial membrane potential and respiratory capacity, which further induced oxidative stress, autophagy, and inflammation [20,21], and finally caused increased apoptosis of neurons and Schwann cells, axonal degeneration, and regeneration disorders [13,22]. Emerging evidences indicate that regulation of AMPK signaling may serve as an attractive therapeutic approach for DPN [8,23–25].

Though few treatment options are accessible, traditional Chinese medicine (TCM) provide potential avenue in DPN management during decades. JinMaiTong (JMT), a formula based on TCM theory, is prescribed at the Peking Union Medical College Hospital to treat DPN successfully. Previous randomized controlled trial showed that JMT significantly relieved symptoms, including numbness, pain, and uncomfortable paresthesia in the limbs, and improved nerve conduction velocity in patients with DPN [26]. JMT has been shown to have good clinical efficacy, safety, and tolerability for over 30 years. The pharmacological mechanism of JMT needs to be further elucidated so as to promote its further use. Our untargeted metabolomics study using an ultra-high-performance liquid chromatography-tandem mass spectrometry (UPLC-MS/MS) platform preliminarily indicated that JMT could ameliorate metabolic disorders in the serum of diabetic rats, among which metabolites closely related to the TCA cycle were involved [27]. However, the specific effects of JMT on central carbohydrate metabolism and energy homeostasis, as well as the underlying molecular mechanisms, have not been clarified.

This study consisted of human, animal, and cellular experiments (Fig. 1). To better understand the relationship between energy metabolism and DPN, we developed a targeted metabolomics approach using high-performance ion chromatography-tandem QTRAP^{TM} mass spectrometry (HPIC-QTRAP-MS/MS) to characterize the profile of central carbohydrate metabolism of DPN in patients and streptozotocin (STZ)-induced rats. On this basis, the pharmaceutical effect and underlying mechanism of JMT were investigated *in vivo* and *in vitro*. The results supported our hypothesis that JMT could significantly correct aberrant metabolism and maintain mitochondrial homeostasis via the activation of AMPK, thereby promoting nerve repair and regeneration in DPN rats and protecting Schwann cells from high-glucose damage. To the best of our knowledge, this is the first study to explore the potential mechanism of TCM in the treatment of DPN based on the holistic regulation of energy metabolism, which is crucial for a better understanding of the clinical effect of JMT. This study also proposes a promising treatment strategy for DPN involving the restoration of energy homeostasis.

2. Materials and methods

2.1. Human study

In the human experiment, 32 patients with DPN and 25 age-matched healthy volunteers were recruited from the Peking Union Medical College Hospital (Beijing, China). The modified Toronto Clinical Neuropathy Score (TCNS) [28] and Michigan Diabetic Neuropathy Score (MDNS) [29], two crucial indicators reflected the severity of peripheral nervous symptoms and functions quantitatively, were evaluated for each patient in this study. The scoring details are listed in Tables S1 and S2. Details of the diagnostic criteria, inclusion and exclusion criteria, and clinical characteristics are shown in the Supplementary data (Section S1 and Table S3). In our study, the diagnosis of DPN was confirmed by a reduction in nerve conduction velocity via neuroelectrophysiological testing, which has been recognized as the gold standard for DPN diagnosis. Fasting serum samples were collected from all participants for targeted metabolomics analysis (Supplementary data Section S1). The study was approved by the Ethics Committee of Peking Union Medical College Hospital (Approval No.: ZS-1969) and performed in accordance with the Declaration of Helsinki. Informed consent was obtained from each participant before participation.

2.2. Drugs and reagents

In accordance with our previously reports [27,30], JMT consists of 12 kinds of TCMs, including the seeds of *Cuscuta chinensis* Lam., the seeds of *Ligustrum lucidum* Ait., the herb of *Prunella vulgaris* L., the herb of *Eclipta prostrate* L., the tender stem of *Cinnamomum cassia* Presl., the herb of *Prunus persica* L., the rhizoma of *Corydalis yanhusuo* W.T. Wang, the seeds of *Cassia obtusifolia* L., *Litchi chinensis* Sonn., radix and the rhizoma of *Asarum heterotropiodes* F., *Hirudo nipponica* W., and *Buthus martensii* K. at a mass ratio of 10:10:10:10:10:10:10:30:30:3:3:3 (Table S4). All crude drugs were obtained from Beijing Tong Ren Tang Co., Ltd. (Beijing, China) and authenticated by Prof. Xiaochun Liang (Peking Union Medical College Hospital, Beijing, China) according to the Chinese Pharmacopoeia. The batch numbers of crude drugs are listed in Table S4. Voucher specimens were deposited at the Department of Traditional Chinese Medicine, Peking Union Medical College Hospital, Beijing, China (Fig. S1). The crude drugs were macerated in distilled water for 2 h and refluxed twice with 10-fold water (1:10, *m/V*) for 2 h. After filtration, the JMT decoction was frozen to dry at −50 °C with yield of 19%, and then kept in seal at −80 °C until rat administration. The chemical profile and main components of JMT from the same batch were investigated by high performance liquid chromatography (HPLC)/triple-time-of-flight (TOF) MS analysis in our previous research [27]. The other drugs, chemicals, and reagents are listed in Table S5.

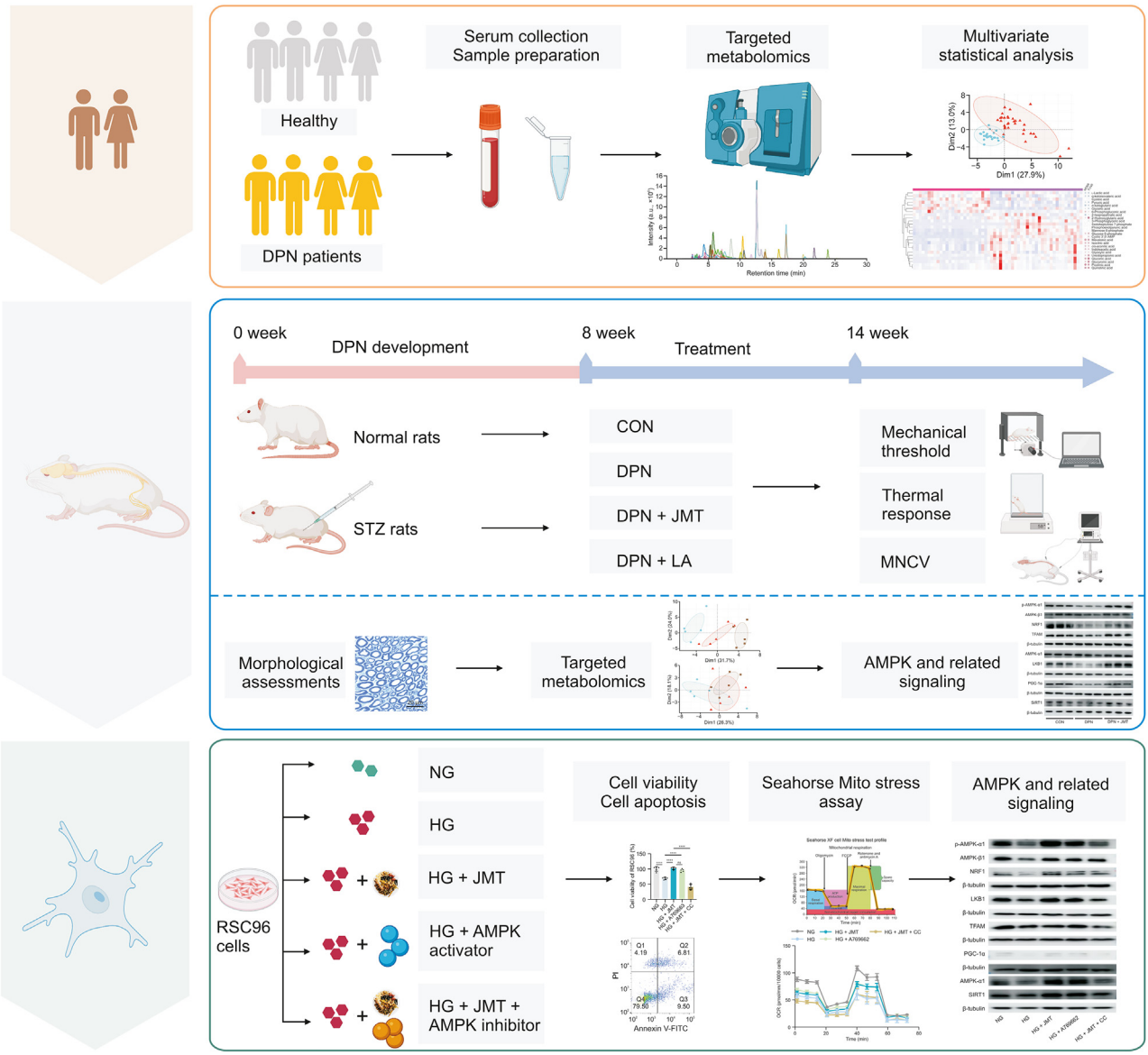

Fig. 1. Schematic overview of the experimental design. This study consisted of human, animal, and cell experiments. $^{****}P < 0.0001$. DPN: diabetic peripheral neuropathy; MDNS: Michigan Diabetic Neuropathy Score; TCNS: modified Toronto Clinical Neuropathy Score; AMP: adenosine monophosphate; CON: control; JMT: JinMaiTong; LA: α-lipoic acid; MNCV: motor nerve conduction velocity; AMPK: AMP-activated protein kinase; NRF1: nuclear respiratory factor 1; TFAM: mitochondrial transcription factor A; LKB1: liver kinase B1; PGC-1α: peroxisome proliferator-activated receptor gamma coactivator 1-alpha; SIRT1: sirtuin 1; NG: normal glucose; HG: high glucose; CC: Compound C (an AMPK inhibitor); PI: propidium iodide; FITC: fluorescein isothiocyanate; OCR: oxygen consumption rate; ATP: adenosine triphosphate; FCCP: carbonyl cyanide-4-(trifluoromethoxy)phenylhydrazone.

2.3. Animal experimental design

Male Sprague-Dawley (SD) rats weighted 180–200 g were purchased from SiPeiFu (Beijing) Biotechnology Co., Ltd. (Beijing, China) and maintained in a specific pathogen-free (SPF) grade environment. Diabetes was induced by a single intraperitoneal injection of 55 mg/kg STZ [31]. Rats with blood glucose >16.7 mmol/L after three days were considered as diabetic models. After eight weeks duration of diabetes, the rats that developed neuropathy confirmed by Von Frey filaments and thermal response tests were randomly assigned to three groups ($n = 6$ per group): DPN model group, DPN treated with JMT group (DPN + JMT), and DPN treated with the positive drug α-lipoic acid (LA, a commonly used drug in the clinic) group (DPN + LA). A control group was established. The rats in the DPN + JMT group were orally administered JMT at a dose of 27.8 g/kg once daily (according to the crude drugs and based on our previous study with various dosages of JMT [27]). The DPN + LA group was treated with LA at a dose of 60 mg/kg daily via gavage. LA was dispersed in 0.5% (*V*/*V*) sodium carboxymethyl cellulose. The control and DPN model rats received the same volume of 0.5% (*V*/*V*) sodium carboxymethyl cellulose. After six weeks of treatment, all rats were sacrificed after the final measurement of behavior and detection of motor nerve conduction velocity (MNCV). Rats were anesthetized with 2% (*V*/*V*) isoflurane (0.41 mL/min at 4 L/min in fresh gas flow), and whole blood samples were obtained from the carotid artery. All rats were sacrificed by exsanguination under deep anesthesia, and sciatic nerves were collected for further experiments.

This study was approved by the Institutional Animal Care and Use Committee of Peking Union Medical College Hospital (Approval No.: XHDW-2022-022), and the experiment were performed in compliance with the Guidelines for the Care and Use of Laboratory Animals issued by the Chinese Council on Animal Research.

2.4. Neurological function tests

2.4.1. Mechanical threshold and thermal response latency

To evaluate the neurological function of the rats, the mechanical pain threshold and thermal response latency were measured every four weeks. The mechanical pain threshold was detected using a Von Frey Pain Measurement Instrument (IITC Life Science Inc., Woodland Hills, CA, USA) as previously described [32]. The thermal response latency was determined using a hot plate apparatus (UGO Basile Inc., Varese, Italy) and tail-flick apparatus (UGO Basile Inc.) following established procedures [33,34].

2.4.2. MNCV

After six weeks of treatment, MNCV was measured using a portable electromyogram-evoked potential instrument (Poseidon Inc., Suzhou, China), as previously described [32]. Briefly, latency (t) was recorded by stimulating the proximal (sciatic notch) and distal (ankle) sites along the sciatic nerve with needle electrodes. The distance (d) between sites was determined. Finally, MNCV was calculated as following: MNCV (m/s) = d/t.

2.5. Sample collection

Blood samples were centrifugated at 3,000 r/min for 10 min, and then serum was isolated and stored at −80 °C for targeted metabolomic analysis. The sciatic nerves on both sides were separated from the rats. The left sciatic nerve was cut into two pieces. One segment (3–4 mm) was fixed in 2.5% (V/V) glutaraldehyde at 4 °C preparing for transmission electronic microscope examination. The other segment was stored at −80 °C for targeted metabolomic analysis. The right sciatic nerve was separated into two sections. One segment was fixed with 4% (V/V) paraformaldehyde (PFA) for pathological examination. The other sample was stored at −80 °C for Western blot. DRG was isolated and fixed with 4% (V/V) PFA for further study.

2.6. Targeted metabolomics analysis

Targeted metabolomic analyses were performed using human sera (n = 32 from patients with DPN and n = 25 from healthy controls), rat sera (n = 5 per group), and rat sciatic nerve tissues (n = 5 per group) to generate comprehensive profiles of central carbohydrate metabolism. Briefly, the metabolomic analysis was performed using a Dionex ICS-6000 HPIC System (Thermo Scientific Inc., San Jose, CA, USA) coupled to a QTRAP™ 6500 triple quadrupole mass spectrometer (AB SCIEX Inc., Foster City, CA, USA). A total of 56 analytes were detected by multiple reaction monitoring (MRM) in the negative mode of the electrospray ionization source. Among these targeted metabolites, half of them were from central carbohydrate metabolism pathways (Nos. 1–28 in Table S6), eight were from other carbohydrate metabolism pathways (Nos. 29–36 in Table S6), 16 were intermediates of amino acid and carbohydrate metabolism (Nos. 37–52 in Table S6), and others were mainly related to nucleotide metabolism (Nos. 53–56 in Table S6). All the metabolites were quantified by calibration curves established with standard solutions. Details for preparation of samples and standard solutions, instrument parameters, method validation, and metabolites quantification were given in Supplementary data (Sections S2–S5).

2.7. Morphological assessments

Morphological changes in sciatic nerves were evaluated using hematoxylin and eosin (H&E) staining, toluidine blue staining, and transmission electron microscopy (TEM) examination.

2.7.1. H&E staining

H&E staining was performed following standard protocols and images were captured using a Zeiss Axioscan slide scanner (Zeiss Inc., Oberkochen, Germany).

2.7.2. Toluidine blue staining

As previously described, abnormally myelinated axons are characterized by demyelination, axonal atrophy, disordered myelin sheaths, and myelin vacuolization [35]. Abnormal myelinated axons were manually counted and calculated as percentages (abnormal axons/total axons).

2.7.3. TEM

The ultrastructures of the mitochondria and myelin sheaths were observed and assessed using TEM (JEOL Inc., Tokyo, Japan). TEM was performed as previously described [35]. Morphometric analyses of the TEM images were performed using ImageJ software (version 1.46r; National Institute of Health, Bethesda, MD, USA). Morphological parameters included axon diameter, myelin diameter, and G-ratio (axon diameter/myelin diameter), which can accurately and objectively assess myelin and axon injuries.

2.8. Immunofluorescence

Immunofluorescence staining of myelin and axon proteins was performed on DRG as described previously [30]. Briefly, the slices were incubated overnight with the myelin basic protein (MBP; 1:100, V/V) and neurofilament heavy-chain (NF-H; 1:100, V/V) antibodies. After washing, the slices were incubated with coralite 488-conjugated goat anti-mouse IgG (heavy and light chains) (1:300, V/V), coralite 594-conjugated goat anti-rabbit IgG (heavy and light chains) (1:300, V/V), and 4',6-diamidino-2-phenylindole (DAPI, 1:200, V/V). All images were taken by laser-scanning confocal microscope (Nikon Inc., Tokyo, Japan).

2.9. Western blot

Western blot was performed following standard protocols. The following antibodies were used: p-AMPK α1 (1:2000, V/V, rabbit), AMPK-α1 (1:1000, V/V, rabbit), AMPK-β1 (1:5000, V/V, rabbit), PGC-1α (1:5000, V/V, mouse), liver kinase B1 (LKB1; 1:1000, V/V, rabbit), nuclear respiratory factor 1 (NRF1; 1:1000, V/V, rabbit), mitochondrial transcription factor A (TFAM; 1:5000, V/V, rabbit), sirtuin 1 (SIRT1; 1:2000, V/V, mouse), β-tubulin (1:20000, V/V, mouse), and horseradish peroxidase (HRP)-conjugated secondary antibody (1:10000, V/V, goat). Finally, the blots were visualized using an enhanced chemiluminescence (ECL) kit and AI680 multifunctional imaging analysis system (GE Health Care Inc., Pittsburg, PA, USA).

2.10. Cell culture and treatment

Rat Schwann cell line (RSC96) was purchased from Cell Resource Center (Institute of Basic Medical Sciences, Chinese Academy of Medical Sciences, Beijing, China). After resuscitation, RSC96 cells were maintained in 25 mM Dulbecco's modified Eagle's medium (DMEM) supplemented with 10% (V/V) fetal bovine serum (FBS) at 37 °C with 5% (V/V) CO_2. Based on preliminary experiments (Fig. S2), a glucose concentration of 100 mM was selected for high glucose stimulation. The JMT lyophilized powder was dissolved in DMEM at an optimal concentration of 0.05 mg/mL, and the cells were co-treated with JMT and high glucose for 72 h, based on its protective effect on the activity of RSC96 cells exposed to high glucose in the preliminary experiment (Figs. S2 and S3). A-769662 (an AMPK activator) and Compound C (CC, an AMPK inhibitor) were dissolved in dimethyl sulfoxide (DMSO) at

optimal concentrations (Fig. S2). RSC96 cells were randomly divided into five groups: normal glucose (25 mM group; NG), high glucose (100 mM glucose; HG), high glucose + JMT (100 mM glucose and 0.05 mg/mL JMT; HG + JMT), high glucose + A-769662 (100 mM glucose and 10 μM A-769662; HG + A769662), and high glucose + JMT (100 mM glucose, 0.05 mg/mL JMT, and 5 μM CC; HG + JMT + CC) to explore the effect of JMT on AMPK pathway.

2.11. Cell viability assay and flow cytometry analysis

The viability of RSC96 cells was examined using a Cell Counting Kit (CCK-8). Apoptosis was detected using an Annexin V-fluorescein isothiocyanate (FITC)/propidium iodide (PI) co-staining kit according to manufacturer's instructions. Briefly, the cells were collected and resuspended in binding buffer at 500 cells/μL. Then the cells were stained with 5 μL of Annexin V-FITC and PI in the dark for 5 min. The flow cytometry gating strategy was illustrated in Fig. S4. All samples were analyzed using a BD flow cytometer (BD Biosciences Inc., San Diego, CA, USA) and FlowJo software (version 10; Ashland, OR, USA).

2.12. ATP content assay

The intracellular ATP concentration was detected by an ATP assay kit. After treatment with the drugs for 72 h, RSC96 cells in 6-well plates were collected using 40 μL of lysate. The samples were then centrifuged at 12,000 *g* at 4 °C for 5 min. The supernatant and ATP standards were respectively mixed with detection solution in black 96-well plates. The luminescence was measured using microplate reader with a luminometer module.

2.13. Mitochondrial membrane potential test and mitochondrial ultra-structure observation

2.13.1. Mito-tracker chloromethyl-X-rosamine (CMXRos) staining

Mito-tracker CMXRos staining was performed to evaluate the mitochondrial membrane potential of the RSC96 cells. Cells were seeded at a density of 1.0×10^5 cells/well in 6-well plates, which were plated a cell-climbing slice at the bottom. After treatment for 72 h, cells were incubated with Mito-tracker Red CMXRos at 37 °C for 30 min, fixed with 4% (*V*/*V*) PFA, and permeabilized with 0.1% (*V*/*V*) Triton X-100. The cells were then incubated with Tubulin-tracker Green (1:50, *V*/*V*) at room temperature in the dark for 1 h and DAPI (1:200, *V*/*V*) for 10 min. Finally, the climbing slices were transferred to glass slides. Images were captured using a laser-scanning confocal microscope (Nikon Inc., Tokyo, Japan).

2.13.2. TEM

The mitochondrial ultrastructure of RSC96 cells was observed by TEM. A total of 3.5×10^5 RSC96 cells were planted and cultured in T25 flasks. The cells were then treated for 72 h, digested with trypsin, and centrifugated at 1,000 r/min for 5 min. After centrifugation, cells were fixed with 2.5% (*V*/*V*) glutaraldehyde. The samples were then encapsulated in agarose and fixed with an osmic acid solution. Following dehydration, the sample was embedded in epoxy resin and cut into 70-nm slices. After staining with uranyl acetate and lead citrate, the ultrastructure of the mitochondria was examined using TEM. Abnormal mitochondria are characterized by vacuolation, crista disruption, and decreased matrix density. The mitochondrial density and percentage of abnormal mitochondria (abnormal mitochondria/total mitochondria) were then calculated [36].

2.14. Mitochondrial respiration assay

To evaluate mitochondrial respiratory function, the oxygen consumption rate (OCR) was measured using a Seahorse XF Cell Mito stress test kit with an XFe 96 extracellular Fluz analyzer (Agilent Technologies Inc., Santa Clara, CA, USA). RSC96 cells were plated on an XF96 cell culture microplate and treated with the drugs for 72 h. Before detection, the sensor cartridge was hydrated in Seahorse XF Calibrant in a non-CO_2 incubator at 37 °C overnight. The assay medium was prepared using Seahorse XF DMEM supplemented with 25 mM glucose, 4 mM glutamine, and 1 mM pyruvate. After being washed and incubated with assay medium, the cells were stimulated by the following reagents: 1.5 μM Oligomycin, 1.0 μM carbonyl cyanide-4-(trifluoromethoxy)phenylhydrazone (FCCP), and 0.5 μM rotenone/antimycin A. OCR was recorded using an XFe 96 extracellular flux analyzer. Subsequently, the cells were labeled with Hoechst 33342 for 20 min. Cell counting was performed using a BioTek Cytation 7 (BioTek Instruments Inc., Winooski, VT, USA). The OCR was normalized to the cell numbers.

2.15. Statistical analysis

All data are expressed as means ± standard deviation (SD). Statistical significance between two groups was assessed using unpaired two-tailed Student's *t*-test, whereas multiple comparisons were evaluated using ordinary one-way analysis of variance (ANOVA). Differences were considered to be significant at $P < 0.05$. Images and blots were quantified using ImageJ software. For metabolomics data, principal component analysis (PCA), heatmap and cluster gram analysis, and Spearman correlation were plotted using https://www.bioinformatics.com.cn (last accessed on May 12, 2023). Pathway enrichment was conducted using MetaboAnalyst 5.0 (https://www.metaboanalyst.ca/home.xhtml). Other statistical analyses and plotting were carried out on the GraphPad Prism software (version 9.3.1; Bethesda, MD, USA).

3. Results

3.1. Targeted metabolomics revealed the distinctive signatures of central carbohydrate metabolism in patients with DPN and STZ-induced DPN rats

To obtain a panoramic view of the metabolic features associated with central carbohydrate metabolism in the circulation and the peripheral nervous system following DPN, a targeted metabolomic approach was developed using the HPIC-QTRAP-MS/MS platform. A total of 56 metabolites were simultaneously determined within a 25-min run (Fig. 2A). Standard curves were established with $r^2 \geq 0.995$ for all analytes (Table S7). The recovery rates were in the range of 83.7%–115.2% with RSDs < 5.0%, and the intra-day RSDs were less than 5.32%, indicating the accuracy and precision were satisfactory for further analysis (Table S7). The stability of these metabolites was acceptable with RSDs ≤ 12.2% within two days at 4 °C (Table S7). The matrix effects of human serum, rat serum, and rat sciatic nerve tissue were 81.7% ± 3.6%, 87.9% ± 4.0%, and 88.6% ± 2.5%, respectively, which were evaluated by the internal standard, hippuric acid-D5. The established method was then applied to analyze human serum (Fig. 2B), rat serum (Fig. 2C), and rat peripheral nerve tissues (Fig. 2D) from different groups.

In human serum samples, 41 targeted metabolites were successfully quantified (Table S8). Unsupervised PCA was conducted to elucidate the metabolic profiles of patients with DPN and healthy subjects, which were readily differentiated (Fig. 2E). The variations in all metabolites are shown in Fig. 2F. In total, 25 metabolites

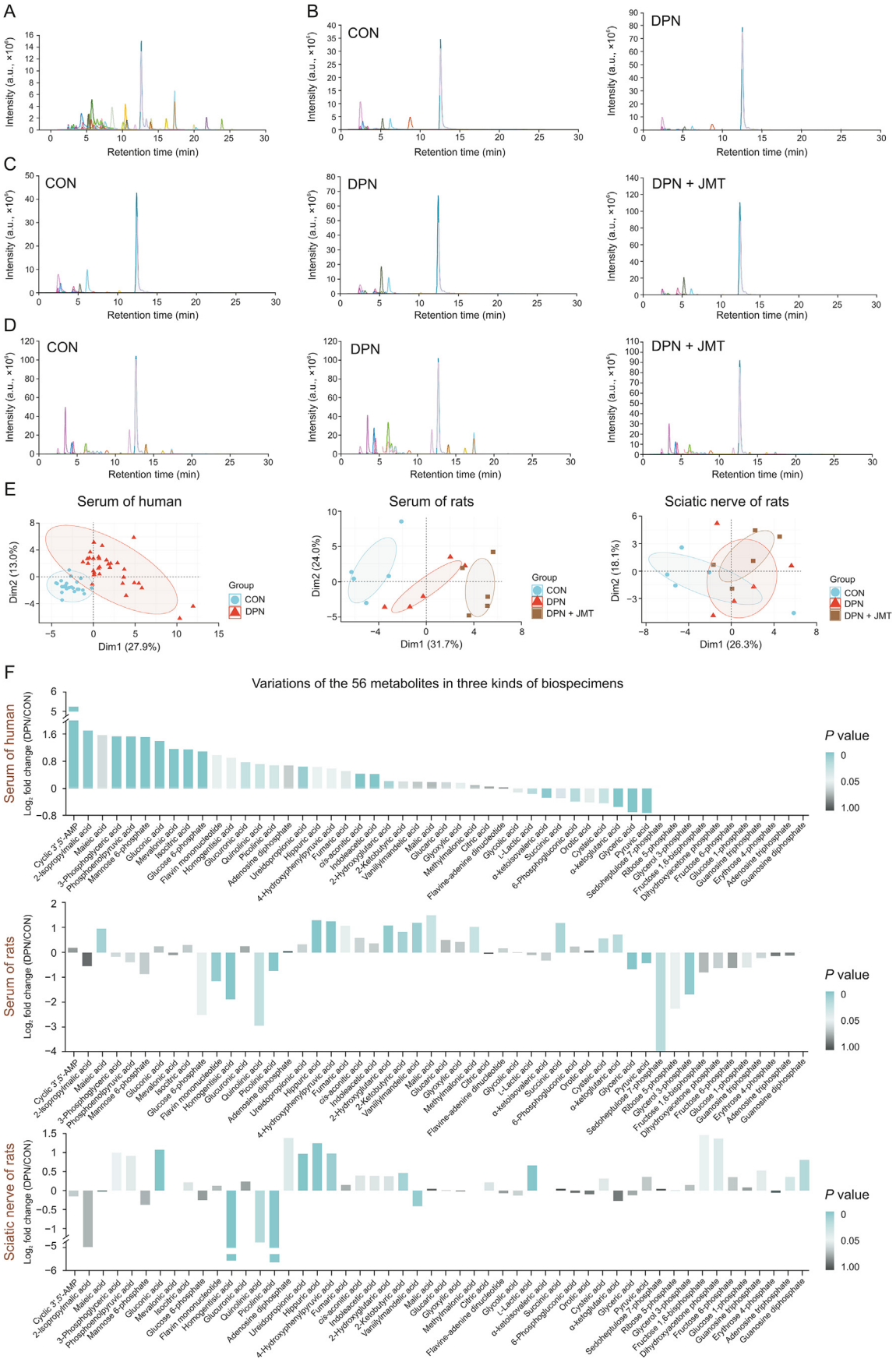
A
B
CON
DPN
C
CON
DPN
DPN + JMT
D
CON
DPN
DPN + JMT
Intensity (a.u., ×10^6)
Retention time (min)
E
Serum of human
Serum of rats
Sciatic nerve of rats
Dim1 (27.9%)
Dim2 (13.0%)
Dim1 (31.7%)
Dim2 (24.0%)
Dim1 (26.3%)
Dim2 (18.1%)
Group
CON
DPN
DPN + JMT
F
Variations of the 56 metabolites in three kinds of biospecimens
Serum of human
Serum of rats
Sciatic nerve of rats
Log2 fold change (DPN/CON)
P value
0
0.05
1.00
Cyclic 3',5'-AMP
2-Isopropylmalic acid
Maleic acid
3-Phosphoglyceric acid
Phosphoenolpyruvic acid
Mannose 6-phosphate
Gluconic acid
Mevalonic acid
Isocitric acid
Glucose 6-phosphate
Flavin mononucleotide
Homogentisic acid
Glucuronic acid
Quinolinic acid
Picolinic acid
Adenosine diphosphate
Ureidopropionic acid
Hippuric acid
4-Hydroxyphenylpyruvic acid
Fumaric acid
cis-Aconitic acid
Indoleacetic acid
2-Hydroxyglutaric acid
2-Ketobutyric acid
Vanillylmandelic acid
Malic acid
Glucaric acid
Glycolic acid
Methylmalonic acid
Citric acid
Flavine-adenine dinucleotide
Glycolic acid
α-Ketoisovaleric acid
L-Lactic acid
Succinic acid
6-Phosphogluconic acid
Orotic acid
Cysteic acid
α-Ketoglutaric acid
Glyceric acid
Pyruvic acid
Sedoheptulose 7-phosphate
Ribose 5-phosphate
Glycerol 3-phosphate
Fructose 1,6-bisphosphate
Dihydroxyacetone phosphate
Fructose 6-phosphate
Glucose 1-phosphate
Guanosine triphosphate
Erythrose 4-phosphate
Adenosine triphosphate
Guanosine diphosphate

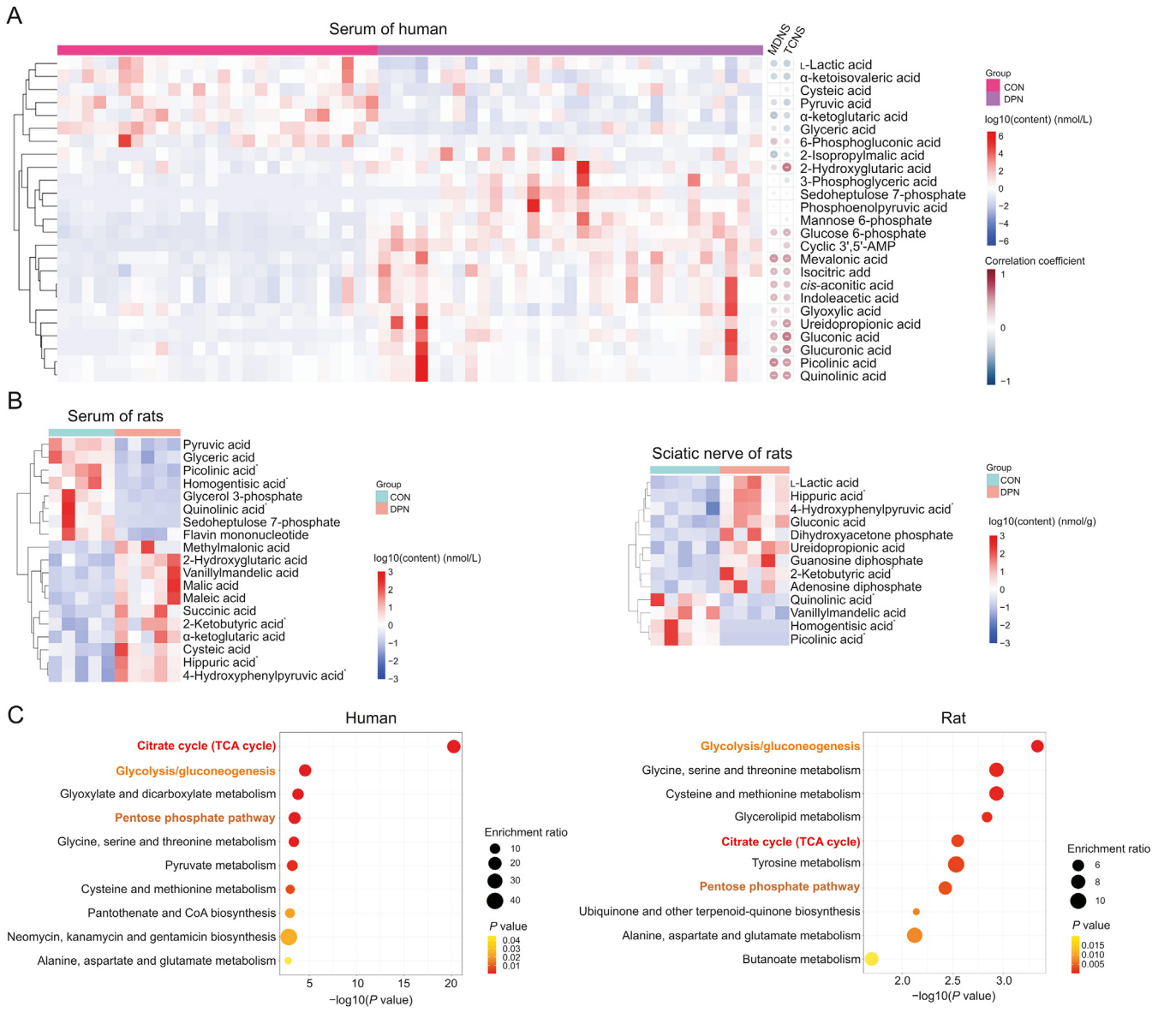

Fig. 3. Heatmaps of metabolites significantly changed in diabetic peripheral neuropathy (DPN). (A) Serum of patients with DPN. (B) Serum and sciatic nerves of rat. (C) Bubble plots of pathway enrichment in human and rats with DPN. Asterisks in B indicate the metabolites significantly changed in both serum and sciatic nerves of rats. * Represents metabolites that significantly changed in both serum and sciatic nerve. $^{*}P < 0.05$ and $^{*}P < 0.01$. MDNS: Michigan Diabetic Neuropathy Score; TCNS: modified Toronto Clinical Neuropathy Score; AMP: adenosine monophosphate; CON: control; TCA: tricarboxylic acid.

showed significant changes (18 increased and 7 decreased) in patients with DPN when compared to the controls ($P < 0.05$), the contents of which were visualized using a heat map (Fig. 3A). Among them, glucose 6-phosphate, cyclic 3',5'-AMP, mannose 6-phosphate, isocitric acid, and glyceric acid were the five most significant metabolites with $P < 1 \times 10^{-6}$.

For the rat samples, 52 and 50 metabolites were detected in the serum and sciatic nerve tissues, respectively (Table S8). PCA score plots revealed distinct clusters of central carbohydrate metabolism in DPN rats and controls, especially in the serum samples (Fig. 2E). Notably, these energy substrates showed not exactly the same variation tendencies in circulation and the peripheral nervous system (Fig. 2F). The contents of 19 and 13 metabolites were significantly different between the groups in the serum and sciatic nerves, respectively ($P < 0.05$; Fig. 3B). Among these, six metabolites were remarkably elevated (2-ketobutyric acid, hippuric acid, and 4-hydroxyphenylpyruvic acid) or reduced (picolinic acid, homogentisic acid, and quinolinic acid) in both serum and sciatic nerves of the DPN rats.

Kyoto encyclopedia of genes and genomes (KEGG) pathway analysis revealed a striking enrichment of the TCA cycle in the serum of patients with DPN, and the following top two pathways included glycolysis/gluconeogenesis and the pentose phosphate pathway (Fig. 3C). In addition, associations between the serum levels of 25 differential metabolites and two clinical indicators that reflect the severity of neurological symptoms and function, MDNS

Fig. 2. Characterization of the aberrant central carbohydrate metabolism in patients with diabetic peripheral neuropathy (DPN) and DPN rats via targeted metabolomics analysis using high-performance ion chromatography-tandem mass spectrometry (HPIC-MS/MS). (A–D) Extracted ion chromatograms (EICs) of the mixed standard references and specimens: the mixed standard references (A), human serum (B), rat serum (C), and rat sciatic nerve (D). (E) Score plots of principal component analysis. (F) Fold-changes and *P* values of all targeted metabolites in different specimens. CON: control; JMT: JinMaiTong; AMP: adenosine monophosphate.

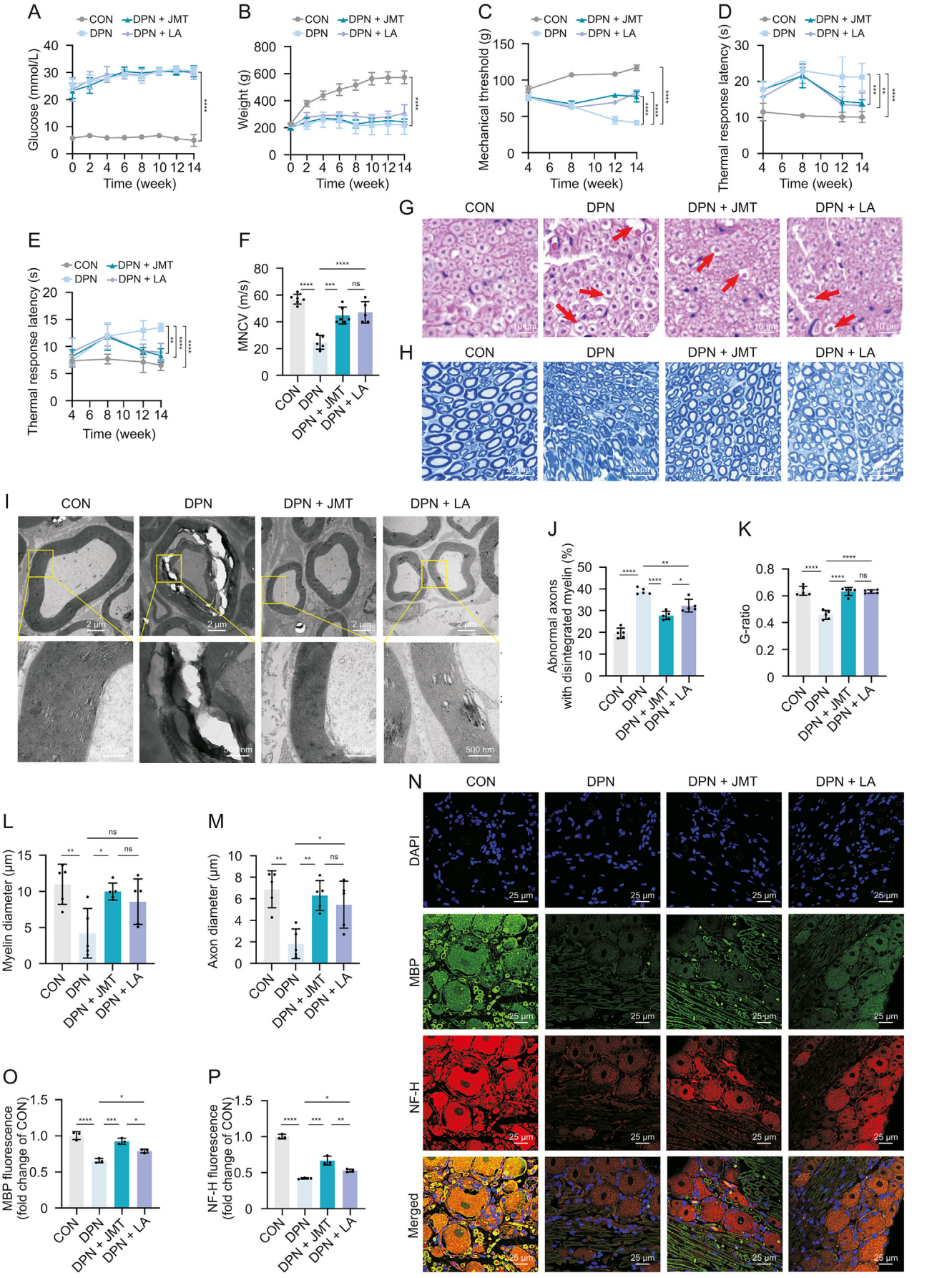
A
CON
DPN
DPN + JMT
DPN + LA
Glucose (mmol/L)
Time (week)
B
Weight (g)
Time (week)
C
Mechanical threshold (g)
Time (week)
D
Thermal response latency (s)
Time (week)
E
Thermal response latency (s)
Time (week)
F
MNCV (m/s)
G
H
I
J
Abnormal axons with disintegrated myelin (%)
K
G-ratio
L
Myelin diameter (μm)
M
Axon diameter (μm)
N
DAPI
MBP
NF-H
Merged
O
MBP fluorescence (fold change of CON)
P
NF-H fluorescence (fold change of CON)

and TCNS, were evaluated in patients with DPN by Spearman correlation. Nine metabolites were significantly correlated with MDNS and/or TCNS ($P < 0.05$), including metabolites related to the TCA cycle (α-ketoglutaric acid, 2-isopropylmalic acid, isocitric acid, and *cis*-aconitic acid), glycolysis (glucose-6-phosphate), and the pentose phosphate pathway (mevalonic acid; Figs. 3A, S5, and S6). In DPN rats (combining the differential metabolites in both the circulatory and peripheral nervous systems), glycolysis was the most enriched pathway, and the TCA cycle also appeared in the top five enriched pathways (Fig. 3C). Together, our data revealed the clinical relevance of DPN phenotypes and disturbed energy metabolism and demonstrated the holistic energy-metabolic landscapes that are apparently disturbed in patients with DPN and rodent models, thus providing a new perspective for the pharmacological study of TCM in the treatment of DPN.

3.2. JMT improved peripheral neurological functions in DPN rats

Next, we investigated the peripheral neuroprotective effect of JMT and explored the pharmacological mechanism of JMT in the regulation of energy homeostasis. The dose of JMT in this study was equivalent to two-fold the clinical dose, which is in accordance with the optimal dose used in our previous study using DPN rats [27]. After STZ injection, rats showed persistent and significant increase in blood glucose levels compared to healthy controls during the experiment (Figs. 4A and S7A). The body weights of STZ-induced rats remarkably decreased since the 2nd week (Figs. 4B and S7B). As shown in Fig. 1, after eight weeks of hyperglycemia, STZ-induced diabetic rats exhibited significant and continuous behavioral changes, including decreased mechanical pain threshold (measured using the Von Frey test; Fig. 4C) and increased thermal response latency (measured using the hot plate and tail flick test; Figs. 4D and E), suggesting the presence of the DPN phenotype. Demyelination and axonal damage were also fully developed in the 8th week according to our previous reports using the same model [37]. DPN rats were then administered JMT and the positive control drug LA for six weeks. At the end of the experiment, neither JMT nor LA treatment had a significant effect on blood glucose levels or body weight (Figs. 4A, 4B, and S7). Treatment with JMT and LA both significantly improved the mechanical pain threshold and thermal response latency in rats with DPN (Figs. 4C–E). Moreover, MNCV of untreated DPN rats were lower than that of healthy control rats at 14 weeks post STZ injection (24.80 ± 5.18 vs. 56.92 ± 3.64 m/s, $P < 0.0001$), which was restored by the JMT and LA treatments (Fig. 4F). These results suggest that JMT significantly improves the peripheral neurological functions in DPN rats.

3.3. JMT mitigated morphological changes in the sciatic nerves of DPN rats

Under light microscopy, both H&E (Fig. 4G) and toluidine blue-stained (Fig. 4H) sections showed a clear structure of sciatic nerves with an orderly arrangement of nerve fibers and normal morphology of the myelin sheath and axons in the control group. Sciatic nerves of DPN rats showed obvious demyelination with axonal shrinkage. Under a transmission electron microscope, the ultrastructure of the myelin lamella of the myelinated fibers of the sciatic nerves was clear in the control group and blurred in the DPN group (Fig. 4I). DPN model rats exhibited marked vacuolar-like defects, separation of lamellae in the myelin sheath, and axonal atrophy, which were improved by JMT. Based on morphometric analysis, the percentage of abnormal axons significantly increased in the DPN group (Fig. 4J), which was markedly decreased by JMT and LA treatment. In addition, untreated DPN rats exhibited a significant reduction in the G-ratio, myelin diameter, and axon diameter when compared with healthy control rats (Figs. 4K–M). JMT significantly improved these morphological changes in the sciatic nerves, suggesting that JMT treatment protected sciatic nerves from diabetic neuropathy-related morphological damage.

3.4. JMT reversed the decrease in myelin and axon protein expression of DPN rats

The myelin sheath in the peripheral nervous system surrounds the axons, and DPN is characterized by demyelination and axonal atrophy [38]. MBP is an important component of the myelin membrane structure [39] and is critical for myelination of nerve fibers [40]. NF-H is an axonal marker associated with axonal atrophy [41]. Therefore, we further examined the expression of MBP and NF-H by immunofluorescence in DRG. MBP was predominantly distributed in myelin sheath and NF-H was highly expressed in the bodies and axons of the neurons (Fig. 4N). The expression of both MBP and NF-H was reduced in DPN model rats, indicating demyelination and regeneration disorders (Figs. 4O and P). Notably, both of them were increased by JMT and LA treatments, and the efficacy of JMT was superior to that of LA. These results suggest that JMT promotes the repair and regeneration of myelin and axons in DPN rats.

3.5. Neuroprotective effect of JMT was related to restoring central carbohydrate metabolism of DPN rats

Considering the aberrant metabolic signatures in DPN and the significant efficacy of JMT, the established metabolomics approach in Section 3.1 was further employed to investigate whether JMT could ameliorate DPN by restoring central carbohydrate homeostasis. As shown in Fig. 2E, the PCA score plots displayed complete separation of rat serum and partial separation of rat sciatic nerves between the DPN and DPN + JMT groups, indicating altered metabolic profiles arising from JMT.

As for the serum samples, nine metabolites were significantly increased and three were decreased in the DPN + JMT group when compared with the DPN model group ($P < 0.05$), while the TCA cycle and pentose phosphate pathway were mainly involved (Figs. 5 and S8). Specifically, JMT robustly elevated the serum concentrations of citric acid in the TCA cycle as well as gluconic acid and glyceric acid in the pentose phosphate pathway. Moreover, JMT greatly augmented the serum levels of ATP and guanosine triphosphate (GTP), two important energy donors that maintain cellular function. Meanwhile, JMT greatly restricted the abnormal accumulation of α-ketoglutaric acid and succinic acid in TCA cycle.

Fig. 4. JinMaiTong (JMT) improved peripheral neurological function and mitigated morphological changes of peripheral nerve in diabetic peripheral neuropathy (DPN) rats. (A, B) Blood glucose level (A) and weight (B) were monitored during the experiment. (C) Mechanical threshold was detected using the Von Frey test every four weeks. (D, E) Thermal response latency was measured using the hot plate (D) and tail flick (E) tests every four weeks. (F) Motor nerve conduction velocity (MNCV) was evaluated after six weeks of treatment with JMT. (G, H) Hematoxylin and eosin (H&E) (G) and toluidine blue (H) staining revealed that the sciatic nerves of DPN rats exhibited disordered arrangement of nerve fibers and demyelination with severe vacuolation and axonal atrophy (red arrow). (I) The ultra-structure of sciatic nerve was observed via transmission electron microscopy (TEM). DPN group showed myelin lamellar separation, vacuolar degeneration, and shrunken axon. Treatment with JMT and α-lipoic acid (LA) mitigated the morphological alterations. (J–M) Morphometric parameters, including abnormal axons with disintegrated myelin (J), G-ratio (axon diameters/myelin diameters) (K), myelin diameters (L), and axon diameters (M), were calculated. (N–P) The representative images (N) of immunofluorescent staining and the proteins levels of myelin basic protein (MBP) (O) and neurofilament heavy-chain (NF-H) (P) were evaluated. Data are expressed as means ± standard deviation (SD). $^{*}P < 0.05$, $^{**}P < 0.01$, $^{***}P < 0.001$, and $^{****}P < 0.0001$. ns: no significant difference. CON: control; DAPI: 4′,6-diamidino-2-phenylindole.

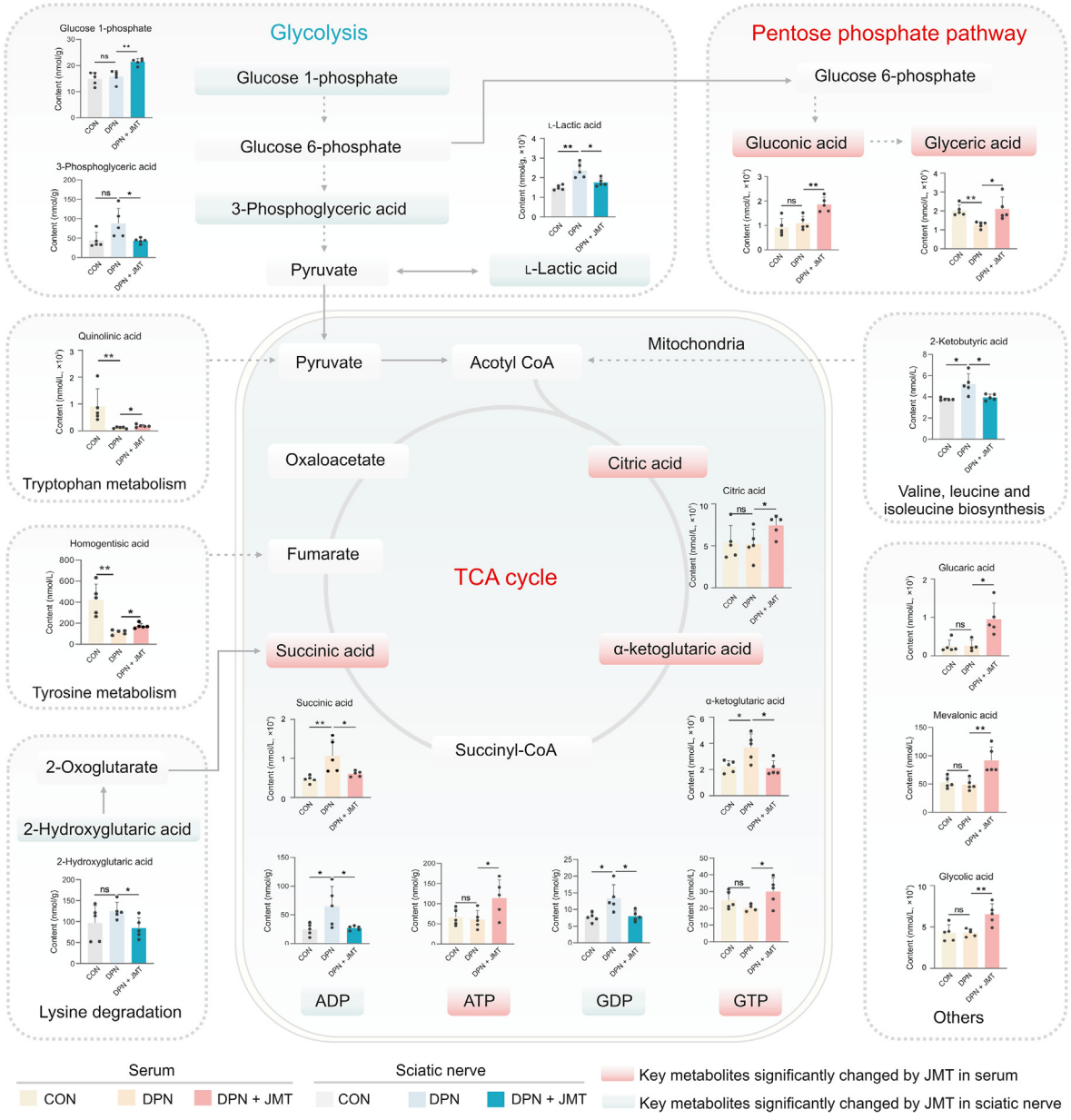

Fig. 5. JinMaiTong (JMT) treatment restored the perturbed central carbohydrate metabolism in the circulation and sciatic nerve of diabetic peripheral neuropathy (DPN) rats. Dash line arrows indicate the direct metabolic reactions, and solid line arrows indicate the indirect reactions. $^{*}P < 0.05$ and $^{**}P < 0.01$. ns: no significant difference. CON: control; TCA: tricarboxylic acid cycle; ADP: adenosine diphosphate: ATP: adenosine triphosphate; GDP: guanosine diphosphate; GTP: guanosine triphosphate.

In the sciatic nerve tissues, seven metabolites showed significant differences in content between the DPN and DPN + JMT groups, three of which were intermediates of the glycolytic pathway (Figs. 5 and S8). In particular, the significant increase in levels of glucose 1-phosphate, as well as the decrease in levels of 3-phosphoglyceric acid and L-lactic acid, indicated that the saturated glycolytic pathway caused by high glucose levels was relieved by JMT treatment. In addition, the abnormal accumulation of 2-hydroxyglutaric acid and 2-ketobutyric acid (two precursors of metabolites in the TCA cycle), as well as ADP and guanosine diphosphate (GDP) in DPN conditions, was remarkably decreased by JMT treatment, implying possible resurgence of the TCA cycle in the mitochondria.

Furthermore, Spearman correlation analyses indicated that 10 JMT called-back metabolites (five from the sciatic nerve and five from circulation) presented moderate to strong correlations ($0.55 \leq |r| \leq 0.82$, $P < 0.05$) with DPN phenotypes (MNCV, mechanical threshold, and/or thermal response latency), including intermediate and end product of glycolysis (Fig. S9), and intermediates of the TCA cycle (Fig. S10). Collectively, these findings indicate that after 6-weeks treatment with JMT, the disorders of central carbohydrate metabolism were corrected to a great extent in both the circulation and peripheral nervous system of DPN rats, which could contribute to the therapeutic effect of JMT. These results support our hypothesis that JMT can improve DPN by restoring perturbed bioenergetics through metabolic crosstalk. Thus, we next sought to disclose the intracellular signaling pathway that JMT mainly acted on to regulate key energy metabolism in peripheral nerves, with the goal of augmenting our understanding of the pharmacological mechanism of JMT in DPN.

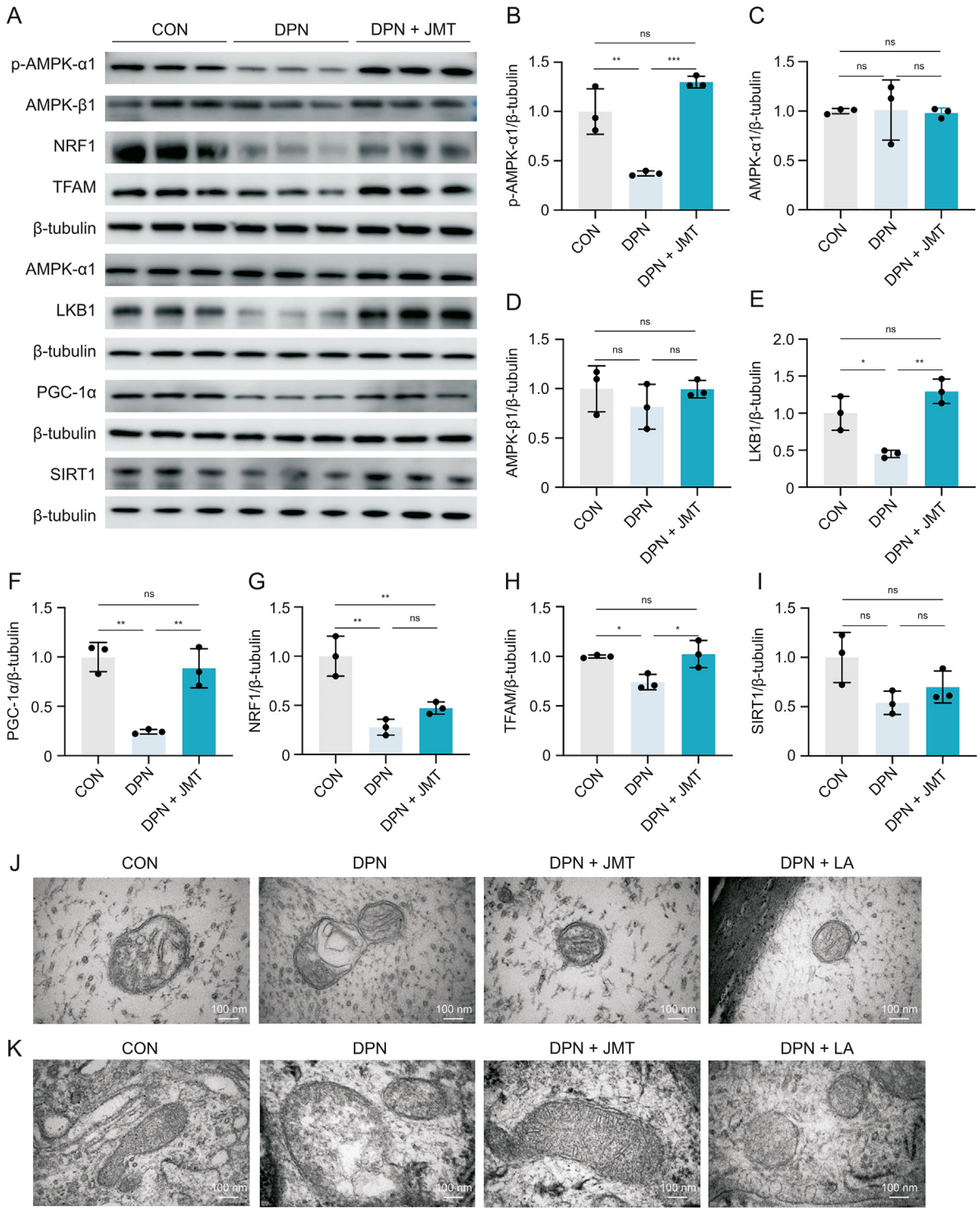

Fig. 6. JinMaiTong (JMT) activated the adenosine monophosphate (AMP)-activated protein kinase (AMPK) signaling pathway and mitigated ultrastructural damages of mitochondria in sciatic nerves (SNs) of diabetic peripheral neuropathy (DPN) rats. (A–I) Western blot analyses of proteins in AMPK signaling pathway (A) including p-AMPK-α1 (B), AMPK-α1 (C), AMPK-β1 (D), liver kinase B1 (LKB1) (E), peroxisome proliferator-activated receptor gamma coactivator 1-alpha (PGC-1α) (F), nuclear respiratory factor (NRF1) (G), mitochondrial transcription factor A (TFAM) (H), and sirtuin 1 (SIRT1) (I) in sciatic nerves from rats in each group. (J, K) Mitochondria in sciatic nerves of DPN rats exhibited mitochondrial vacuolation, swelling, fragmentation, cristate loss, and decreased matrix density under transmission electron microscopy (TEM), which were attenuated by JMT and α-lipoic acid (LA): mitochondria in axon of sciatic nerve (J) and mitochondria in Schwann cell of sciatic nerve (K). Data are expressed as means ± standard deviation (SD). $^{*}P < 0.05$, $^{**}P < 0.01$, and $^{***}P < 0.001$. ns: no significant difference. CON: control.

3.6. JMT activated the AMPK/PGC-1α signaling pathway in vivo

AMPK is the primary conductor in maintenance of energy homeostasis in the peripheral nervous system [6]. Therefore, we speculated that the regulation of energy metabolism by JMT could be mediated by AMPK. We further examined the effect of JMT on AMPK and its influence on upstream and downstream proteins in the sciatic nerves using Western blot. As shown in Figs. 6A and B,

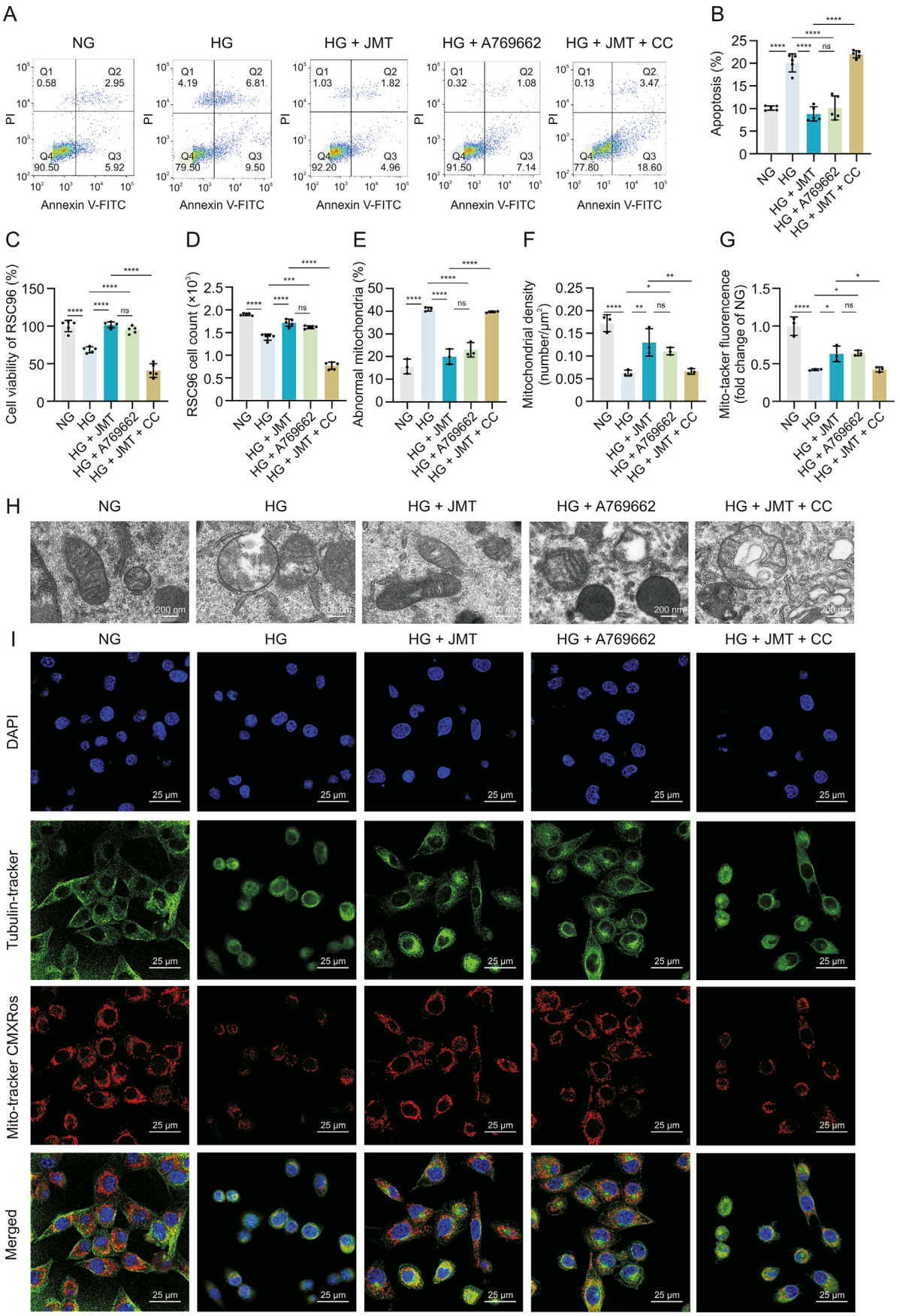
A
NG
HG
HG + JMT
HG + A769662
HG + JMT + CC
Q1 0.58
Q2 2.95
Q4 90.50
Q3 5.92
Q1 4.19
Q2 6.81
Q4 79.50
Q3 9.50
Q1 1.03
Q2 1.82
Q4 92.20
Q3 4.96
Q1 0.32
Q2 1.08
Q4 91.50
Q3 7.14
Q1 0.13
Q2 3.47
Q4 77.80
Q3 18.60
PI
Annexin V-FITC
B
Apoptosis (%)
C
Cell viability of RSC96 (%)
D
RSC96 cell count (×10³)
E
Abnormal mitochondria (%)
F
Mitochondrial density (number/μm²)
G
Mito-tacker fluorencence (fold change of NG)
H
200 nm
I
DAPI
Tubulin-tracker
Mito-tracker CMXRos
Merged
25 μm

DPN rats exhibited a significant decrease in phosphorylated AMPK-α1 (p-AMPK-α1) expression compared to non-diabetic controls, while there were no significant differences in AMPK-α1 and AMPK-β1 levels between the control and DPN groups (Figs. 6A, C, and D). These results suggested that chronic hyperglycemia interfered the phosphorylation of AMPK-α1 and JMT promoted AMPK phosphorylation in the sciatic nerves of DPN rats (Figs. 6A and B). Furthermore, JMT stimulated the expression of LKB1, an upstream activator of AMPK, which was reduced in the DPN group (Figs. 6A and E).

Then, we analyzed the protein level of PGC-1α, which was the downstream of AMPK and the key transcription coactivator responsible for mitochondrial biogenesis. The protein level of PGC-1α was significantly reduced in the DPN group compared to controls (Figs. 6A and F), which was markedly elevated by JMT administration. Additionally, we analyzed the expressions of TFAM and NRF1, the down-stream targets of PGC-1α, which played important roles in mitochondrial structure and function [42]. Both NRF1 and TFAM levels were significantly reduced in the DPN group (Figs. 6A, G, and H). JMT significantly upregulated the expression of TFAM but had no significant effect on NRF1. SIRT1 has been reported to increase PGC-1α expression, thus regulating mitochondrial function. Therefore, we examined the expression of SIRT1, and no significant difference was observed between the DPN and healthy control rats (Figs. 6A and I). Taken together, JMT treatment activated LKB1-AMPK-PGC-1α and the downstream TFAM in DPN rats, which could affect the mitochondrial structure and function.

3.7. JMT mitigated mitochondrial morphological damage in vivo

We further investigated the effects of JMT on the morphology and structure of mitochondria. As shown in Figs. 6J and K, the ultrastructure of the mitochondria in sciatic nerves was observed by TEM. In the control group, the mitochondria exhibited normal morphology with double membrane contours and clear cristae. Mitochondria in the axons and Schwann cells in the DPN model group showed a blurred membrane structure and cristae, swelling, membrane destruction, and vacuolar-like defects, indicating mitochondrial degeneration. These morphological changes were reversed in JMT-treated group (Figs. 6J and K).

3.8. JMT promoted the proliferation and suppressed the apoptosis of RSC96 cells exposed to high-glucose via AMPK

Schwann cells support and protect neurons, nourish axons, and promote cell survival and growth after nerve injury. Schwann cell dysfunction is widely recognized in the pathogenesis of DPN [41,43]. To investigate whether the neuroprotective effect of JMT was mediated by AMPK, we used an AMPK inhibitor. The Annexin V-FITC/PI co-staining kit was used to test the apoptosis, and the CCK-8 assay was used to assess cell proliferation of RSC96 cells exposed to high-glucose (Figs. 7A–C). As shown in Fig. 7C, high glucose significantly inhibited the proliferation of RSC96 cells, which was reversed by JMT treatment. In addition, the efficacy of JMT was comparable to that of the AMPK activator A769662. Notably, the effect of JMT on RSC96 cells was inhibited by co-culture with the AMPK inhibitor CC. Flow cytometry analysis demonstrated that high glucose exposure resulted in a substantial increase in the apoptotic population (Figs. 7A and B), which was accompanied by a decrease in the number of RSC96 cells (Fig. 7D). Treatment with JMT decreased apoptosis and increased the number of RSC96 cells, indicating that JMT protected RSC96 cells against high glucose. Moreover, co-treatment with JMT and CC showed no significant effect on the apoptosis and cell count of RSC96 cells at high glucose concentrations, indicating that the effects of JMT were associated with the activation of AMPK.

3.9. JMT attenuated the morphological changes and respiratory dysfunction of mitochondria in RSC96 cells exposed to high-glucose via AMPK

We further investigated the effect of JMT on mitochondrial ultrastructure and mitochondrial membrane potential in RSC96 cells exposed to high glucose (Figs. 7E–I). In NG group, the mitochondria had a regular size, distinct cristae, and an intact double membrane, whereas the mitochondria of RSC96 cells in HG group exhibited enlargement, swelling, vacuolar degeneration, and crista rupture (Fig. 7H). In particular, JMT treatment significantly mitigated these abnormal ultrastructural alterations in RSC96 cells exposed to high-glucose, which were eliminated by co-treatment with an AMPK inhibitor. Subsequent morphometric analyses revealed that the HG group displayed a marked increase in the percentage of abnormal mitochondria and reduction in mitochondrial density. JMT treatment significantly reduced the percentage of abnormal mitochondria and increased mitochondrial density, which was equal to that of the AMPK activator. Notably, these effects were inhibited by co-treatment with the AMPK inhibitor, CC (Figs. 7E and F). In addition, high-glucose exposure caused a decrease in the mitochondrial membrane potential in RSC96 cells compared to that in the NG group. JMT significantly increased the mitochondrial membrane potential of RSC96 cells cultured in high-glucose, but this effect was inhibited by co-treatment with CC (Figs. 7G and I).

The mitochondrial OCR is the most important parameter for testing mitochondrial respiratory function and activity and was further measured using an extracellular Fluz analyzer to evaluate the effect of JMT on mitochondrial function in live RSC96 cells exposed to high glucose. Compared with the NG group, the HG group showed lower basal respiration OCR, maximal respiration OCR, and spare respiratory capacity, indicating bioenergetic alterations in RSC 96 cells exposed to high glucose (Figs. 8A–E). Among these parameters, JMT treatment significantly restored the maximal respiration OCR and spare-respiratory capacity, suggesting that JMT enhanced the reserve ability of respiratory function under energy stress induced by high glucose. Moreover, the effect of JMT on maximal respiration was markedly attenuated by the AMPK inhibitor CC. Simultaneously, ATP production in RSC96 cells was significantly suppressed by high glucose and significantly upregulated by JMT treatment. However, co-treatment with JMT and CC had no effect on ATP production (Fig. 8F).

3.10. Inhibition of AMPK abolished the activated effect of JMT on downstream PGC-1α in RSC96 cells exposed to high-glucose

The expression of AMPK/PGC-1 α signaling proteins was evaluated in RSC96 cells cultured under high-glucose conditions (Figs. 8G–O). Exposure of high glucose significantly suppressed the

Fig. 7. JinMaiTong (JMT) relieved high-glucose induced injury of rat Schwann cell line (RSC96). (A–D) Apoptosis (A, B), cell viability (C), and the number of RSC96 cells (D) were determined. (E–G) The abnormal mitochondrial percentage (E), mitochondrial density (F), and mitochondrial membrane potential (G) was evaluated. (H) The representative images of mitochondria in RSC96 cells under transmission electron microscopy (TEM). (I) The representative images of mitochondria in RSC96 cells by Mito-tracker chloromethyl-X-rosamine (CMXRos) immunofluorescent staining. Data are expressed as means ± standard deviation (SD). $^{*}P < 0.05$, $^{**}P < 0.01$, $^{***}P < 0.001$, and $^{****}P < 0.0001$. ns: no significant difference. PI: propidium iodide; FITC: fluorescein isothiocyanate; NG: normal glucose; HG: high glucose; CC: Compound C (an adenosine monophosphate (AMP)-activated protein kinase (AMPK) inhibitor); DAPI: 4′,6-diamidino-2-phenylindole.

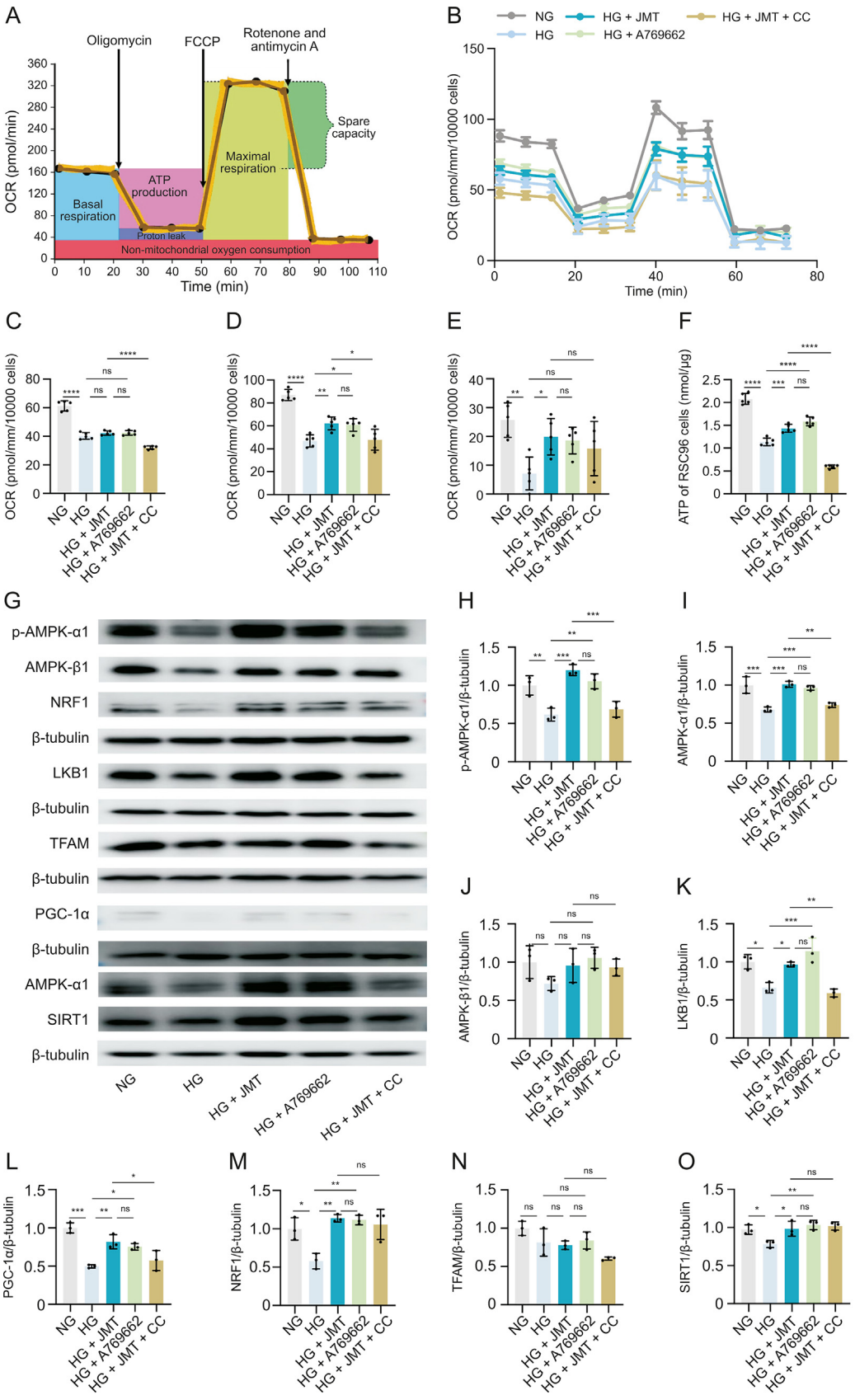

Fig. 8. Mitochondrial respiratory function and expression of adenosine monophosphate (AMP)-activated protein kinase (AMPK)/proliferator-activated receptor gamma coactivator 1-alpha (PGC-1α) signaling-related proteins in rat Schwann cell line (RSC96). (A) Mitochondrial respiratory function was determined using the Seahorse XF Cell Mito stress test kit. (B) Oxygen consumption rate (OCR) was normalized by cell counts. (C–F) Basal respiration OCR (C), maximal respiration OCR (D), spare respiratory capacity (E), and adenosine triphosphate (ATP) (F) of RSC96 cells were measured. (G–O) Western blot analyses of proteins in AMPK signaling pathway (G) including p-AMPK-α1 (H), AMPK-α1 (I), AMPK-β1 (J),

expression of p-AMPK-α1 and AMPK-α1, suggesting an obstruction of phosphorylation of AMPK. JMT treatment remarkably increased the expression of both p-AMPK-α1 and AMPK-α1, given that JMT acted as an agonist of AMPK. Positive effects of JMT on LKB1, PGC-1α, NRF1, and SIRT1 were also observed *in vitro*. Furthermore, the levels of relevant signaling molecules were determined after AMPK inhibition. It is worth noting that the elevation of PGC-1α, the downstream of AMPK, induced by JMT treatment was abolished by inhibiting AMPK. These data not only confirmed the *in-vivo* results that JMT could activate AMPK under diabetic conditions, but also further revealed that these effects could act on Schwann cells and mainly contribute to the AMPK/PCG-1α axis.

4. Discussion

DPN is a serious complication of diabetes that leads to a decline in quality of life and an increase in mortality. Abnormal energy metabolism has been implicated in the pathogenesis of DPN [3]. However, the introduction of metabolomics-targeted central carbohydrate metabolism has been lacking to further illustrate the energy status as well as metabolic crosstalk in DPN. In this setting, we developed a HPIC-MS/MS method to obtain the most comprehensive description of central carbohydrate metabolism by simultaneously targeting 56 metabolites. For determination of these highly polar substances, HPIC solves the shortcomings of poor reservation in reversed phase HPLC and simplifies the experimental process without derivatization. With its unique selectivity, some studies have successfully coupled HPIC with MS for qualitative and quantitative detection of metabolites such as carbohydrates, sugar phosphates, organic acids, and nucleotides in biological samples [44,45]. Additionally, the HPIC-MS method also displayed high sensitivity with detection limit as low as 0.07 nmol/L at a signal-to-noise ratio of 3 in this study. Overall, we further demonstrated the superior resolution and sensitivity of HPIC for the challenging analysis of polar compounds in complex biological matrices.

Using this UPIC-MS/MS approach, metabolic perturbations in serum of patients were panoramically mapped for the first time. Moreover, correlations between metabolic dysfunction and clinical neuropathic symptoms were successfully established in our study, further implying the involvement of energy dysfunction in DPN progression. In addition, a previous study revealed that, in an experimental diabetic neuropathy rat model, metabolic dysfunction was restricted to the sciatic nerve rather than the DRG or trigeminal ganglia [12]. Therefore, sciatic nerve tissue and serum samples from an STZ-induced DPN rat model and controls were analyzed using the same approach. As a result, the disturbances in central carbohydrate metabolism in the sciatic nerve were of some similarities to those in circulation. Six metabolites were abnormally expressed in both the serum and sciatic nerves of the DPN rats (Fig. 3B, metabolites with asterisk). Although the metabolic profiles were not identical among species, the centerpiece of energetic dysfunction was the TCA cycle and glycolysis in the serum of both humans and rats with DPN (Fig. S11). Several studies have also revealed that glycolysis and the TCA cycle are two metabolic pathways that are severely affected by hyperglycemia and further contribute to the onset and development of DPN [11,12].

Our data also indicated that the energy substrates did not show the same variation tendencies in the circulation and sciatic nerves of DPN rats, as the primary altered pathway was the TCA cycle in the circulation, whereas excessive glycolysis was mainly displayed in the sciatic nerve. The metabolic differences in serum and sciatic nerve of DPN rats revealed the specific susceptibilities of peripheral nerve to holistic metabolic disorders. Nevertheless, among the 19 and 13 differential expressed metabolites, there were six ones (noted with asterisk in Fig. 3B) showed the same variation tendences in serum and nerve tissue. Taken together, these findings suggest a complicated interaction between systemic and nerve-specific metabolic processes. The importance of energy-metabolic disorders and tissue-specific metabolism in the pathogenesis of DPN still warrant further exploration. Our unprecedented metabolomics study offers a reliable and substantial resource to recognize the aberrant details of energy homeostasis in DPN in a systematic view, thereby offering an important basis for further development of therapeutic strategies for DPN.

JMT is a TCM formula prescribed by Peking Union Medical College Hospital. It has been used clinically for decades and has demonstrated reliable efficacy [26]. Our previous studies revealed that JMT displayed a satisfactory neuroprotective effect following prophylactic administration (starting from the onset of diabetes) [27,30,37]. The current study is the first to demonstrate that the therapeutic administration of JMT (starting at the 9th week after diabetes, when the DPN model was fully developed [37]) also significantly improved peripheral neurological functions and alleviated neuropathological damage, including demyelination and axon degeneration, in the sciatic nerves of DPN rats. Furthermore, we found that JMT remarkably increased the protein expression of MBP and NF-H and that the main proteins formed myelin and axons, indicating that JMT promoted neural repair and regeneration. Our results indicate that JMT has a better effect than LA on the repair of myelin and axons.

To identify the metabolites underlying the relieved DPN phenotype induced by JMT, sciatic nerve tissue and serum samples of rats from different groups were profiled using the targeted metabolomics platform established above. JMT regulated multiple aberrations in energy metabolism. Pathway analysis identified glycolysis as the most altered pathway in DPN rats compared to normal controls (Fig. 3C). Meanwhile, the dominant role of JMT in the sciatic nerve was the suppression of excessive glycolysis, marked by a significant reduction in 3-phosphoglyceric acid and L-lactic acid. In Particular, the levels of these two metabolites showed the most significant correlation with DPN phenotypes (Fig. S9). Although glycolysis within a certain range supports the injured axons, excessive glycolysis leads axons to degenerate [43,46]. Abnormal accumulation of L-lactic acid, the end product of glycolysis, causes lactate acidosis associated with neurological manifestations [47]. Coincidentally, it has been supposed that the manipulation of glycolytic activity in Schwann cells may constitute a promising therapeutic strategy for relieving DPN [43]. Moreover, elevated lactic acid level is considered as an indicator of mitochondrial dysfunction [48]. In this study, elevated levels of TCA-derived organic acids that suggested the blocking of TCA cycle, such as α-ketoglutaric acid and succinic acid, were observed mainly in the serum of DPN rats and were substantially reduced after JMT treatment. Another finding of the present study was the increased levels of ATP induced by JMT, both *in vivo* and *in vitro*. Prolonged failure of ATP generation ultimately leads to axonal degeneration and disorders in myelin regeneration, while elevation of ATP concentration confers neuroprotection [3,6]. Collectively, our results demonstrate that JMT might alleviate DPN via the integrative regulation of energy homeostasis,

liver kinase B1 (LKB1) (K), PGC-1α (L), nuclear respiratory factor 1 (NRF1) (M), mitochondrial transcription factor A (TFAM) (N), and sirtuin 1 (SIRT1) (O) in RSC96 cells. Data are expressed as means ± standard deviation (SD). $^{*}P < 0.05$, $^{**}P < 0.01$, $^{***}P < 0.001$, and $^{****}P < 0.0001$. ns: no significant difference. FCCP: carbonyl cyanide-4-(trifluoromethoxy) phenylhydrazone; NG: normal glucose; HG: high glucose; JMT: JinMaiTong; CC: Compound C (an AMPK inhibitor).

thereby inviting a more comprehensive perspective on the approach to antagonize DPN.

AMPK serves as a cellular energy sensor and master controller that maintains energy homeostasis. Impaired AMPK signaling contributes to metabolic alterations and mitochondrial dysfunction in peripheral nerve neurons, leading to the onset and development of DPN [6,7]. AMPK activation was shown to rescue mitochondrial deficits and further ameliorate autophagy impairment, oxidative stress, and neuroinflammation in a DPN model [21]. Moreover, LKB1 is a key upstream mediator of AMPK phosphorylation [49]. Abundant evidence indicates that decreased LKB1 and AMPK expression induces demyelination and neuronal damage in DPN [25,50]. LKB1 deletion in Schwann cells can perturb the bioenergetics and metabolic support for axons, leading to axonal degeneration [51]. The activation of LKB1 has been reported to prevent peripheral nerve injury from diabetes-induced oxidative stress by decreasing apoptosis and increasing autophagy [52]. Therefore, based on these studies and our data, it is reasonable to believe that the neuroprotective effects of JMT may be attributed to the activation of AMPK and LKB1.

PGC-1α, the downstream of AMPK, is the key transcription coactivator responsible for mitochondrial respiration and biogenesis. It has been reported that knockdown of PGC-1α in diabetic mice contributes to severe mitochondrial dysfunction and degeneration, resulting in the exacerbation of peripheral neuropathy [18]. Under diabetic conditions, the expression of PGC-1α, enzyme

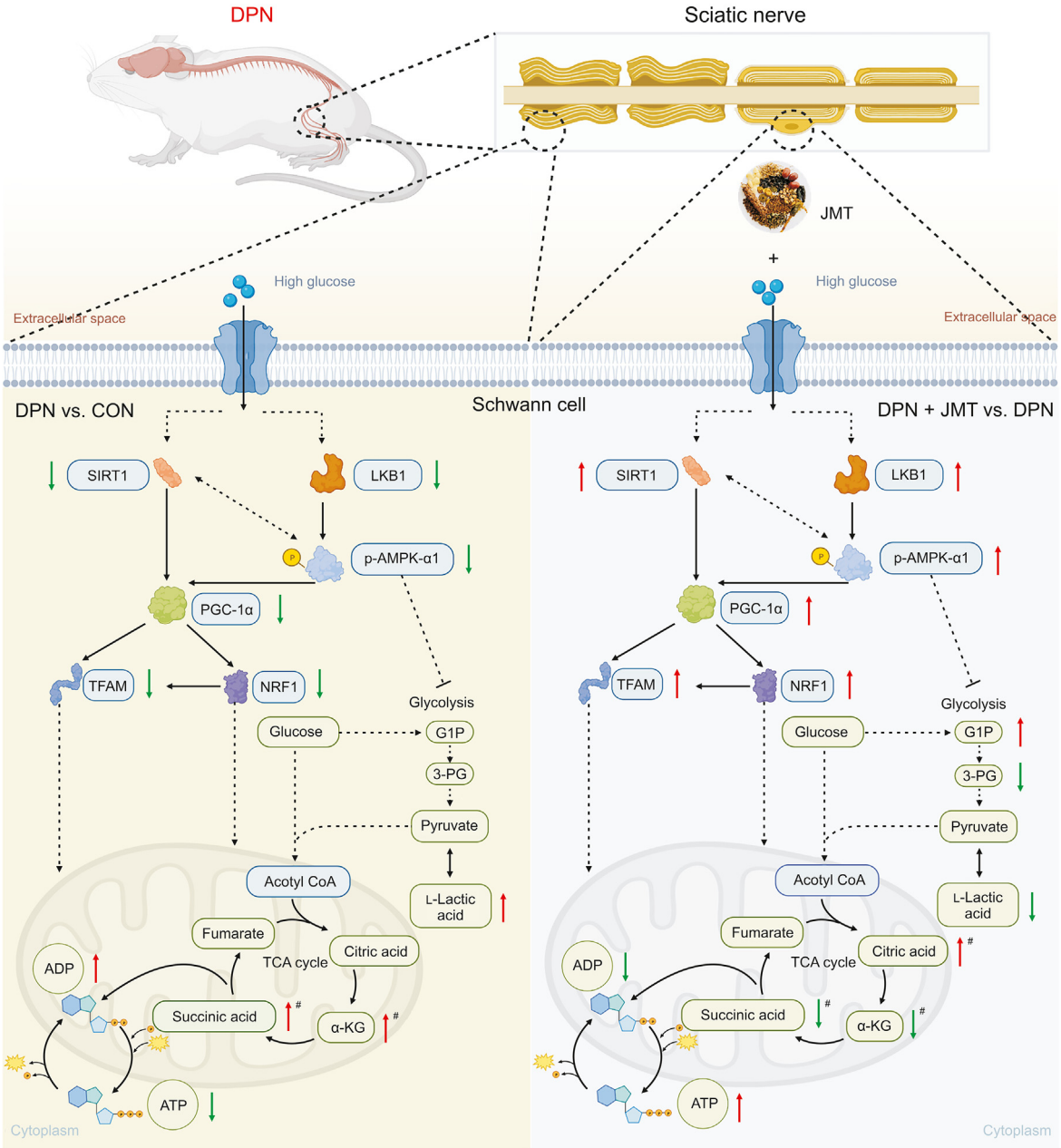

Fig. 9. The neuroprotective effect of JinMaiTong (JMT) on diabetic peripheral neuropathy (DPN) rats via modulating energy homeostasis. # Indicates metabolites with significantly altered contents in rat serum. CON: control. SIRT1: sirtuin 1; LKB1: liver kinase B1; AMPK: adenosine monophosphate (AMP)-activated protein kinase; PGC-1α: proliferator-activated receptor gamma coactivator 1-alpha; TFAM: mitochondrial transcription factor A; NRF1: nuclear respiratory factor 1; G1P: glucose 1-phosphate; 3-PG: 3-phosphoglyceric; α-KG: α-ketoglutaric acid; TCA: tricarboxylic acid cycle; ADP: adenosine diphosphate; ATP: adenosine triphosphate.

activity of the mitochondrial respiratory chain, and bioenergetics profiles are impaired in the sensory neurons of STZ-induced rodents [7]. Upregulation of the AMPK/PGC-1α pathway can promote neurite growth in diabetic rats, thus protecting neurons [7]. Our study observed the suppression of PGC-1α induced by hyperglycemia *in vivo* and *in vitro*, which is supported by previous reports [32]. JMT treatment remarkably elevated the expression level of PGC-1α accompanied with improvement in mitochondrial degeneration, mitochondrial membrane potentials, and metabolic disorders. *In-vitro* study further proved that JMT improved mitochondrial respiratory function and facilitated ATP generation, thus enhancing the adaptability of cells to high glucose toxicity. Moreover, we found that the inhibition of AMPK abolished the activating effect of JMT on PGC-1α, which further suggests that AMPK/PGC-1α signaling pathway is a crucial mechanism for JMT amelioration of DPN.

TFAM and NRF1 are downstream transcription factors of the AMPK/PGC-1α axis, which can be activated by PGC-1α, and in turn enhance mitochondrial respiration [53]. NRF1 and TFAM were previously reported to be significantly downregulated in dorsal root ganglion neurons under diabetic condition [18]. In our study, both were significantly decreased in the sciatic nerves of DPN rats and TFAM was repaired by JMT treatment. SIRT1 is a nicotinamide adenine dinucleotide (NAD^+)-dependent deacetylase that is upregulated by AMPK activation via the elevation of NAD^+ [54]. SIRT1 also can catalyze PGC1-α deacetylation to promote cellular metabolism and restore mitochondrial function in response to high-glucose damage [55]. It was reported that upregulation of SIRT1 preserved mitochondrial function and attenuated diabetic neuropathy [56]. Our results showed that JMT treatment enhanced SIRT1 expression in HG-injured RSC96 cells. These results strongly suggested that JMT stimulated the AMPK activation cascade, which is a promising therapeutic strategy for DPN.

Schwann cells not only form myelin but also provide metabolic and trophic support to neurons and axons. Disruption of the mitochondria in Schwann cells can affect neuronal survival, induce axonal degeneration, and cause peripheral nerve injury [57]. Hyperglycemia has been shown to induce remodeling of the mitochondrial proteome and decrease the efficiency of oxidative phosphorylation in the Schwann cells of peripheral nerves [17]. Our study showed that RSC96 cells cultured with high glucose exhibited obvious mitochondrial respiratory dysfunction and structural damage, with decreased proliferative viability and increased apoptosis. Adverse effects of high glucose on Schwann cells were eliminated by JMT treatment. Moreover, the benefits of JMT on mitochondrial metabolism, proliferation, and apoptosis of Schwann cells under high-glucose conditions were eliminated by an AMPK inhibitor *in vitro*. Therefore, the pharmacological effect of JMT against DPN was attributed to AMPK activation. Taken together, our findings showed that the disturbance of carbohydrate metabolism, mainly glycolysis and the TCA cycle, was widely involved in patients with DPN as well as in STZ-induced DPN rats. The TCM formula JMT ameliorated DPN independent of blood glucose *in vivo* and *in vitro*. Mechanistically, the activation of AMPK signaling was, at least in part, responsible for the regulation of energy status and mitochondrial function, which further promoted nerve repair, even after full-blown demyelination and axonal damage. Fig. 9 shows a holistic view of JMT's role in DPN rats.

Some components in JMT, such as the exact of *Ligustrum vulgare*, *Prunella vulgaris*, and *Cassia artemisiodes*, have been reported to improve diabetes-induced neuropathic pain in rodent models [58–60]. Our previous study revealed the chemical composition of JMT decoction using a UPLC-MS/MS method, indicating that the dominant compounds in JMT mainly included flavonoids, triterpenoids, phenolic acid, and their glycosides [27]. Some flavonoids identified from JMT, including quercetin, kaempferol, luteolin, hesperidin, apigenin, and scutellarin, have been reported to relieve peripheral neuropathy *in vivo* [32,61–64]. Ursolic acid, a main triterpenoid also found in JMT, has been found to promote myelin repair in central nervous system [63]. Notably, a few of components in JMT, especially some flavonoids with neuroprotective activities, have been found to play a key role in regulating energy homeostasis. Our previous study has found that quercetin improved mitochondrial dysfunction and activated AMPK signaling in peripheral nerve under diabetic condition [32]. Also, it has been reported that kaempferol, salidroside, and chlorogenic acid could maintain energy homeostasis by restoring TCA cycle [65–67]. Aside from these known compounds, we believe that the effect of JMT in regulating energy metabolism should be the integrative role of multiple components, which needs more exploration in further study.

One limitation of the current study is the absence of an in-depth target validation of the JMT. Nevertheless, synergistic effect of multicomponents and multitargets has been supposed as the core reason for TCMs to exert their clinical efficacy [68,69]. As our metabolomic analysis revealed from clinical to animal models, the perturbed metabolic network of DPN involves multiple pathways. JMT displayed integrative regulation of central carbohydrate metabolism, which could have advantages in the management of DPN. Our research suggests that JMT can be an effective therapy and that manipulation of energy homeostasis is a promising approach for the treatment of DPN. Furthermore, the key bioactive compounds in this formula are yet to be elucidated to accelerate the acceptance and application of JMT.

5. Conclusions

In this study, an HPIC-MS/MS based metabolomics approach targeted 56 endogenous metabolites surrounding central carbohydrate metabolism were successfully developed and applied in patients with DPN and STZ-induced DPN rats, which provided novel insights into the molecular pathology of DPN. Our study further proved the TCM formula JMT as an effective therapy for treatment of DPN, which improved the neurological functions and attenuated the pathological damages of peripheral nerve in the progress phase of DPN rats. *In-vivo* and *in-vitro* studies demonstrated that the neuroprotective capacities of JMT should be attributed to the improved energy status with vital role of the activated AMPK signaling. Our study suggests that integrated modulation of energy metabolism using TCM can provide effective strategies for treatment of DPN.

CRediT author statement

Bingjia Zhao: Investigation, Data curation, Writing - Original draft preparation; **Qian Zhang:** Conceptualization, Funding acquisition, Writing - Reviewing and Editing; **Yiqian He** and **Weifang Cao:** Investigation; **Wei Song:** Methodology, Data curation, Writing - Reviewing and Editing; **Xiaochun Liang:** Project administration, Supervision.

Declaration of competing interest

The authors declare that there are no conflicts of interest.

Acknowledgments

This work was supported by the National Natural Science Foundation of China (Grant Nos.: 82104827 and 82274336), the National High Level Hospital Clinical Research Funding, China

(Grant No.: 2022-PUMCH-A-265), and the Young Elite Scientists Sponsorship Program by China Association of Chinese Medicine (Grant No.: CACM-2022-QNRC2-B14). Figs. 1 and 9 were created with Biorender.com.

Appendix A. Supplementary data

Supplementary data to this article can be found online at https://doi.org/10.1016/j.jpha.2023.09.007.

References

[1] M.A. Elafros, H. Andersen, D.L. Bennett, et al., Towards prevention of diabetic peripheral neuropathy: Clinical presentation, pathogenesis, and new treatments, Lancet Neurol. 21 (2022) 922–936.
[2] D. Selvarajah, D. Kar, K. Khunti, et al., Diabetic peripheral neuropathy: Advances in diagnosis and strategies for screening and early intervention, Lancet Diabetes Endocrinol. 7 (2019) 938–948.
[3] E.L. Feldman, K.A. Nave, T.S. Jensen, et al., New horizons in diabetic neuropathy: Mechanisms, bioenergetics, and pain, Neuron 93 (2017) 1296–1313.
[4] A. Sadosky, J. Mardekian, B. Parsons, et al., Healthcare utilization and costs in diabetes relative to the clinical spectrum of painful diabetic peripheral neuropathy, J. Diabetes Complications 29 (2015) 212–217.
[5] H. Tang, A. Jiang, J. Ma, et al., Understanding the signaling pathways related to the mechanism and treatment of diabetic peripheral neuropathy, Endocrinology 160 (2019) 2119–2127.
[6] P. Fernyhough, Mitochondrial dysfunction in diabetic neuropathy: A series of unfortunate metabolic events, Curr. Diabetes Rep. 15 (2015), 89.
[7] S.K. Roy Chowdhury, D.R. Smith, A. Saleh, et al., Impaired adenosine monophosphate-activated protein kinase signalling in dorsal root ganglia neurons is linked to mitochondrial dysfunction and peripheral neuropathy in diabetes, Brain 135 (2012) 1751–1766.
[8] Y.V. Madhavi, N. Gaikwad, V.G. Yerra, et al., Targeting AMPK in diabetes and diabetic complications: Energy homeostasis, autophagy and mitochondrial health, Curr. Med. Chem. 26 (2019) 5207–5229.
[9] B.L. Tang, Glucose, glycolysis, and neurodegenerative diseases, J. Cell. Physiol. 235 (2020) 7653–7662.
[10] A.V. Mathew, M. Jaiswal, L. Ang, et al., Impaired amino acid and TCA metabolism and cardiovascular autonomic neuropathy progression in type 1 diabetes, Diabetes 68 (2019) 2035–2044.
[11] D.R. Rojas, R. Kuner, N. Agarwal, Metabolomic signature of type 1 diabetes-induced sensory loss and nerve damage in diabetic neuropathy, J. Mol. Med. 97 (2019) 845–854.
[12] O.J. Freeman, R.D. Unwin, A.W. Dowsey, et al., Metabolic dysfunction is restricted to the sciatic nerve in experimental diabetic neuropathy, Diabetes 65 (2016) 228–238.
[13] S.K. Chowdhury, D.R. Smith, P. Fernyhough, The role of aberrant mitochondrial bioenergetics in diabetic neuropathy, Neurobiol. Dis. 51 (2013) 56–65.
[14] S.K. Chowdhury, E. Zherebitskaya, D.R. Smith, et al., Mitochondrial respiratory chain dysfunction in dorsal root ganglia of streptozotocin-induced diabetic rats and its correction by insulin treatment, Diabetes 59 (2010) 1082–1091.
[15] S. Srinivasan, M. Stevens, J.W. Wiley, Diabetic peripheral neuropathy: Evidence for apoptosis and associated mitochondrial dysfunction, Diabetes 49 (2000) 1932–1938.
[16] E. Akude, E. Zherebitskaya, S.K. Chowdhury, et al., Diminished superoxide generation is associated with respiratory chain dysfunction and changes in the mitochondrial proteome of sensory neurons from diabetic rats, Diabetes 60 (2011) 288–297.
[17] L. Zhang, C. Yu, F.E. Vasquez, et al., Hyperglycemia alters the Schwann cell mitochondrial proteome and decreases coupled respiration in the absence of superoxide production, J. Proteome Res. 9 (2010) 458–471.
[18] J. Choi, K. Chandrasekaran, T. Inoue, et al., PGC-1α regulation of mitochondrial degeneration in experimental diabetic neuropathy, Neurobiol. Dis. 64 (2014) 118–130.
[19] J.D. Panes, A. Wendt, O. Ramirez-Molina, et al., Deciphering the role of PGC-1α in neurological disorders: From mitochondrial dysfunction to synaptic failure, Neural Regen. Res. 17 (2022) 237–245.
[20] V.G. Yerra, A. Areti, A. Kumar, Adenosine monophosphate-activated protein kinase abates hyperglycaemia-induced neuronal injury in experimental models of diabetic neuropathy: Effects on mitochondrial biogenesis, autophagy and neuroinflammation, Mol. Neurobiol. 54 (2017) 2301–2312.
[21] V.G. Yerra, A.K. Kalvala, B. Sherkhane, et al., Adenosine monophosphate-activated protein kinase modulation by berberine attenuates mitochondrial deficits and redox imbalance in experimental diabetic neuropathy, Neuropharmacology 131 (2018) 256–270.
[22] S.K. Chowdhury, R.T. Dobrowsky, P. Fernyhough, Nutrient excess and altered mitochondrial proteome and function contribute to neurodegeneration in diabetes, Mitochondrion 11 (2011) 845–854.
[23] Q. Yuan, X. Zhang, W. Wei, et al., Lycorine improves peripheral nerve function by promoting Schwann cell autophagy via AMPK pathway activation and MMP9 downregulation in diabetic peripheral neuropathy, Pharmacol. Res. 175 (2022), 105985.
[24] X. Xu, W. Wang, Z. Wang, et al., DW14006 as a direct AMPKα activator ameliorates diabetic peripheral neuropathy in mice, Diabetes 69 (2020) 1974–1988.
[25] X. Zhu, Y. Chen, X. Xu, et al., SP6616 as a Kv2.1 inhibitor efficiently ameliorates peripheral neuropathy in diabetic mice, EBioMedicine 61 (2020), 103061.
[26] X. Liang, L. Cui, S. Guo, Clinical study on Jinmaitong composita on diabetic peripheral neuropathy, Zhongguo Zhong Xi Yi Jie He Za Zhi 19 (1999) 517–519.
[27] Q. Zhang, W. Song, X. Liang, et al., A metabolic insight into the neuroprotective effect of Jin-Mai-Tong (JMT) decoction on diabetic rats with peripheral neuropathy using untargeted metabolomics strategy, Front. Pharmacol. 11 (2020), 221.
[28] V. Bril, S. Tomioka, R.A. Buchanan, et al., Reliability and validity of the modified Toronto Clinical Neuropathy Score in diabetic sensorimotor polyneuropathy, Diabet. Med. 26 (2009) 240–246.
[29] E.L. Feldman, M.J. Stevens, P.K. Thomas, et al., A practical two-step quantitative clinical and electrophysiological assessment for the diagnosis and staging of diabetic neuropathy, Diabetes Care 17 (1994) 1281–1289.
[30] J. Xie, W. Song, X. Liang, et al., Jinmaitong ameliorates diabetic peripheral neuropathy in streptozotocin-induced diabetic rats by modulating gut microbiota and neuregulin 1, Aging 12 (2020) 17436–17458.
[31] B.L. Furman, Streptozotocin-induced diabetic models in mice and rats, Curr. Protoc. Pharmacol. 70 (2015), 5.47.1–5.47.20.
[32] Q. Zhang, W. Song, B. Zhao, et al., Quercetin attenuates diabetic peripheral neuropathy by correcting mitochondrial abnormality via activation of AMPK/PGC-1α pathway *in vivo* and *in vitro*, Front. Neurosci. 15 (2021), 636172.
[33] A. Othman, R. Bianchi, I. Alecu, et al., Lowering plasma 1-deoxysphingolipids improves neuropathy in diabetic rats, Diabetes 64 (2015) 1035–1045.
[34] T. Masuda, Y. Ozono, S. Mikuriya, et al., Dorsal horn neurons release extracellular ATP in a VNUT-dependent manner that underlies neuropathic pain, Nat. Commun. 7 (2016), 12529.
[35] B. Zhao, Q. Zhang, X. Liang, et al., Quercetin reduces inflammation in a rat model of diabetic peripheral neuropathy by regulating the TLR4/MyD88/NF-κB signalling pathway, Eur. J. Pharmacol. 912 (2021), 174607.
[36] C. Mollinari, C. De Dominicis, L. Lupacchini, et al., Detection of pathological markers of neurodegenerative diseases following microfluidic direct conversion of patient fibroblasts into neurons, Int. J. Mol. Sci. 23 (2022), 2147.
[37] W. Song, Y. Sun, X. Liang, et al., Jinmaitong ameliorates diabetes-induced peripheral neuropathy in rats through Wnt/β-catenin signaling pathway, J. Ethnopharmacol. 266 (2021), 113461.
[38] D.W. Zochodne, H.S. Sun, C. Cheng, et al., Accelerated diabetic neuropathy in axons without neurofilaments, Brain 127 (2004) 2193–2200.
[39] B. Liu, W. Xin, J. Tan, et al., Myelin sheath structure and regeneration in peripheral nerve injury repair, Proc. Natl. Acad. Sci. U S A 116 (2019) 22347–22352.
[40] X. Shi, Y. Chen, L. Nadeem, et al., Beneficial effect of TNF-α inhibition on diabetic peripheral neuropathy, J. Neuroinflammation 10 (2013), 69.
[41] X. Zhang, S. Zhao, Q. Yuan, et al., TXNIP, a novel key factor to cause Schwann cell dysfunction in diabetic peripheral neuropathy, under the regulation of PI3K/Akt pathway inhibition-induced DNMT1 and DNMT3a overexpression, Cell Death Dis. 12 (2021), 642.
[42] J.H. Koh, Y.W. Kim, D.Y. Seo, et al., Mitochondrial TFAM as a signaling regulator between cellular organelles: A perspective on metabolic diseases, Diabetes Metab. J. 45 (2021) 853–865.
[43] E. Babetto, K.M. Wong, B. Beirowski, A glycolytic shift in Schwann cells supports injured axons, Nat. Neurosci. 23 (2020) 1215–1228.
[44] J. Wang, T.T. Christison, K. Misuno, et al., Metabolomic profiling of anionic metabolites in head and neck cancer cells by capillary ion chromatography with Orbitrap mass spectrometry, Anal. Chem. 86 (2014) 5116–5124.
[45] K. Burgess, D. Creek, P. Dewsbury, et al., Semi-targeted analysis of metabolites using capillary-flow ion chromatography coupled to high-resolution mass spectrometry, Rapid Commun. Mass Spectrom. 25 (2011) 3447–3452.
[46] D.R. Tomlinson, N.J. Gardiner, Glucose neurotoxicity, Nat. Rev. Neurosci. 9 (2008) 36–45.
[47] E. Domènech-Estévez, H. Baloui, C. Repond, et al., Distribution of monocarboxylate transporters in the peripheral nervous system suggests putative roles in lactate shuttling and myelination, J. Neurosci. 35 (2015) 4151–4156.
[48] W.T. Regenold, P. Phatak, C.M. Marano, et al., Elevated cerebrospinal fluid lactate concentrations in patients with bipolar disorder and schizophrenia: Implications for the mitochondrial dysfunction hypothesis, Biol. Psychiatry 65 (2009) 489–494.
[49] T. Behl, A. Gupta, A. Sehgal, et al., A spotlight on underlying the mechanism of AMPK in diabetes complications, Inflamm. Res. 70 (2021) 939–957.
[50] J. Yang, Y. Wei, T. Zhao, et al., Magnolol effectively ameliorates diabetic peripheral neuropathy in mice, Phytomedicine 107 (2022), 154434.
[51] B. Beirowski, E. Babetto, J.P. Golden, et al., Metabolic regulator LKB1 is crucial for Schwann cell-mediated axon maintenance, Nat. Neurosci. 17 (2014) 1351–1361.
[52] Y.C. Chung, J.H. Lim, H.M. Oh, et al., Calcimimetic restores diabetic peripheral neuropathy by ameliorating apoptosis and improving autophagy, Cell Death Dis. 9 (2018), 1163.
[53] L. Hao, W. Zhong, H. Dong, et al., ATF4 activation promotes hepatic mitochondrial dysfunction by repressing NRF1-TFAM signalling in alcoholic steatohepatitis, Gut 70 (2021) 1933–1945.

[54] C. Cantó, Z. Gerhart-Hines, J.N. Feige, et al., AMPK regulates energy expenditure by modulating NAD^+ metabolism and SIRT1 activity, Nature 458 (2009) 1056–1060.
[55] K. Chandrasekaran, M. Salimian, S.R. Konduru, et al., Overexpression of Sirtuin 1 protein in neurons prevents and reverses experimental diabetic neuropathy, Brain 142 (2019) 3737–3752.
[56] V.G. Yerra, A.K. Kalvala, A. Kumar, Isoliquiritigenin reduces oxidative damage and alleviates mitochondrial impairment by SIRT1 activation in experimental diabetic neuropathy, J. Nutr. Biochem. 47 (2017) 41–52.
[57] N.P. Gonçalves, C.B. Vægter, H. Andersen, et al., Schwann cell interactions with axons and microvessels in diabetic neuropathy, Nat. Rev. Neurol. 13 (2017) 135–147.
[58] H.L. Seo, S.Y. Baek, E.H. Lee, et al., *Liqustri lucidi* Fructus inhibits hepatic injury and functions as an antioxidant by activation of AMP-activated protein kinase *in vivo* and *in vitro*, Chem. Biol. Interact. 262 (2017) 57–68.
[59] K. Raafat, M. Wurglics, M. Schubert-Zsilavecz, *Prunella vulgaris* L. active components and their hypoglycemic and antinociceptive effects in alloxan-induced diabetic mice, Biomed. Pharmacother. 84 (2016) 1008–1018.
[60] R. Ullah, W. Badshah, G. Ali, et al., Cassia artemisiodes attenuates nociceptive and diabetes-induced neuropathic pain modalities apropos antioxidant and anti-inflammatory mechanisms, Biomed. Pharmacother. 149 (2022), 112834.
[61] L. Kishore, N. Kaur, R. Singh, Effect of Kaempferol isolated from seeds of *Eruca sativa* on changes of pain sensitivity in streptozotocin-induced diabetic neuropathy, Inflammopharmacology 26 (2018) 993–1003.
[62] A.I. Carballo-Villalobos, M.E. González-Trujano, N. Alvarado-Vázquez, et al., Pro-inflammatory cytokines involvement in the hesperidin antihyperalgesic effects at peripheral and central levels in a neuropathic pain model, Inflammopharmacology 25 (2017) 265–269.
[63] M. Kim, J. Jung, N.Y. Jeong, et al., The natural plant flavonoid apigenin is a strong antioxidant that effectively delays peripheral neurodegenerative processes, Anat. Sci. Int. 94 (2019) 285–294.
[64] P. Basu, A. Basu, *In vitro* and *in vivo* effects of flavonoids on peripheral neuropathic pain, Molecules 25 (2020), 1171.
[65] J. Chitturi, V. Santhakumar, S.S. Kannurpatti, Beneficial effects of kaempferol after developmental traumatic brain injury is through protection of mitochondrial function, oxidative metabolism, and neural viability, J. Neurotrauma 36 (2019) 1264–1278.
[66] Z. Xu, X. Chen, X. Jin, et al., SILAC-based proteomic analysis reveals that salidroside antagonizes cobalt chloride-induced hypoxic effects by restoring the tricarboxylic acid cycle in cardiomyocytes, J. Proteomics 130 (2016) 211–220.
[67] S. Takahashi, K. Saito, X. Li, et al., iTRAQ-based quantitative proteomics reveals the energy metabolism alterations induced by chlorogenic acid in HepG2 cells, Nutrients 14 (2022), 1676.
[68] S. Fu, R. Cheng, Z. Deng, et al., Qualitative analysis of chemical components in Lianhua Qingwen capsule by HPLC-Q Exactive-Orbitrap-MS coupled with GC-MS, J. Pharm. Anal. 11 (2021) 709–716.
[69] X. Jiang, Y. Lin, Y. Wu, et al., Identification of potential anti-pneumonia pharmacological components of *Glycyrrhizae Radix* et Rhizoma after the treatment with Gan An He Ji oral liquid, J. Pharm. Anal. 12 (2022) 839–851.